On the uniqueness of intrinsic viscoelastic properties of materials extracted from nanoindentation using FEMU

M.C. Barick[a], Y. Gaillard[a], A. Lejeune[a], F. Amiot[a], F. Richard[a]

[a]Univ. Bourgogne Franche-Comté, Institut FEMTO-ST, CNRS/UFC/ENSMM/UTBM, Département Mécanique Appliquée, 24 rue de l'Epitaphe, 25000 Besançon, France

Abstract

Instrumented nanoindentation is widely used to extract the material properties from the measured force-displacement curves. In this work, the uniqueness/non-uniqueness of the intrinsic viscoelastic properties of materials determined by nanoindentation during load-unload tests is investigated. A four-parameter viscoelastic law with constant Poisson's ratio is used to model the mechanical behavior of a polymer material and a 2D-axisymetric Finite Element Model (FEM) is used to simulate the nanoindentation test. Firstly, a nanoindentation experimental triangular load-unload test is performed on a bulk sample of polypropylene (PP) with a Berkovich indenter tip at a depth rate of 1000 nm/min. The values of the four material parameters are estimated by the Finite Element Model Updating (FEMU). The numerical results can accurately fit the experimental data. However, several quasi-solutions are shown to exist. These load-unload data allow to identify only three viscoelastic parameters if the Poisson's ratio is known. Secondly, the effect of nanoindentation depth rate, loading type (triangular, trapezoidal, exponential, sinusoidal) and apex angle is numerically investigated using an identifiability index based on the conditioning of the inverse problem. We show a correlation between the identifiability index and the energy dissipated by the material during the tests. The extraction of all material parameters remains impossible using a single test. Finally, some combinations of several nanoindentation triangular tests and indenter tip angles are also investigated. We show that a dual nanoindentation technique (cube corner and Berkovich tips) with triangular load-unload tests is an interesting combination to reliably extract all the viscoelastic parameters, provided that plasticity is taken into account. This result illustrates the interest of using this numerical identifiability index to design nanoindentation experiments to ensure the robustness of the intrinsic viscoelastic properties extraction.

Keywords: **Viscoelasticity, Nanoindentation, Polymers, Identifiability, Uniqueness, FEMU.**

1. Introduction

Nanoindentation is a powerful technique for mechanical characterization of polymeric materials at small-scale (Cheng and Cheng, 2004; VanLandingham et al., 2005; Zhang et al., 2006). During the nanoindentation test, a rigid indenter tip is pushed into the surface of a solid and then removed. The force $P(t)$ and the displacement $h(t)$ are continuously recorded during loading and unloading segments. The resulting force–displacement curve is associated to the material properties, the geometry of the sample and the geometry of the indenter tip. Several models have been proposed to retrieve the elastic modulus and the hardness from such experimental data (Doerner and Nix, 1986; Oliver and Pharr, 1992). These methods generally assume that the material features a purely elastic behavior during the unloading part and does not exhibit any loading rate dependence (Oliver and Pharr, 1992). However, most of polymers exhibit a significant viscoelastic behavior (Tang and Ngan, 2003). It is therefore important to develop a method to retrieve the intrinsic viscoelastic properties of a material from the temporal data of such nanoindentation test. Two approaches have thus been proposed in the literature instead of the classical Oliver & Pharr method (Chen et al., 2013). The first approach is based on the viscoelastic contact theory (Lee, 1955; Radok, 1957; Lee and Radok, 1960; Graham, 1965). The dimensional analysis or the Laplace transform method are used to extend the elastic solution to viscoelastic phenomena. The models yield closed-form solutions, which are used to analyze the nanoindentation test. The parameters are obtained by fitting the experimental force–displacement data (Cheng et al., 2000; Vandamme and Ulm, 2006; Liu et al., 2006; Oyen, 2006). These parameters, such as compliance constants and retardation times describe a mechanical system behavior in which the material is involved, but these are not intrinsic to the material. Indeed, these models generally include correction factors, which mix intrinsic material properties with geometrical consideration, to tune the contact conditions. A good example is the β factor which corrects the Sneddon relation of elasticity for non-axisymmetric indentation (Oliver and Pharr, 1992). The vast majority of reported results make use of $\beta = 1.034$ (King, 1987). It is however known that this factor strongly depends on the tested material (Oliver and Pharr, 2004). This furthermore makes these models often over-parameterized, thus leading to multiple solutions for the fitting procedure (Menčík et al., 2011). Converting the properties estimated by this approach should into inputs for structural engineering problems based on the finite element analysis is therefore a difficult and non-obvious task. The second approach is carried out by combining Finite Element Method (FEM) and numerical optimization. In this method, the objective function, which is a norm of difference between the numerical nanoindentation force and/or displacement and experimental data, is minimized using optimization techniques (Qasmi et al., 2004; Guessasma et al., 2008). The parameters of the model are determined as the minimizer of the objective function. However, the uniqueness of this minimizer is generally not assessed in the literature, but it remains a fundamental question, particularly in instrumented nanoindentation. In fact, in the case of elastoplastic behavior, numerous works have shown that a group of materials with distinct elastoplastic properties may yield almost the same conical indentation $P-h$ curve (Cheng and Cheng, 1999; Capehart and Cheng, 2003; Alkorta et al., 2005). It implies that the material properties cannot be uniquely determined by using a single sharp indenter tip. In order to address this problem in the case of elastoplastic behavior, dual or multiple indentation techniques have been proposed by several

authors (Le, 2008; Heinrich et al., 2009; Le, 2011). However, the existence of mystical materials that give almost similar $P-h$ curves for different indenter tips with half angles ranging from 60° to 80° has also been shown (Chen et al., 2007). Recently, this problem of non-uniqueness of the elastoplastic properties was investigated by Phadikar et al. (Phadikar et al., 2013). They found that non-uniqueness of the solution is caused by a high sensitivity to the experimental errors. They also demonstrated that dual nanoindentation techniques are reliable when the experimental error is within $\pm 1\%$. This question is poorly addressed in the presence of viscous phenomena (viscoelastic and/or viscoplastic). Constantinescu and Tardieu (Constantinescu and Tardieu, 2001) highlighted this difficulty in the case of Maxwell and Norton–Hoff behaviors.

In this paper, the uniqueness/non-uniqueness of the viscoelastic properties of materials determined by the Finite Element Model Updating (FEMU) of the nanoindentation test is studied. A four-parameter viscoelastic behavior law with constant Poisson's ratio, which has been implemented in a 2D axisymmetric finite element model of the nanoindentation test, is first described in section 2. Then, the FEMU method used to adjust the force-displacement curves on the experimental data is presented. As an experimental reference, a nanoindentation triangular test at constant depth rate on a PP sample is performed. It is shown in the section 3 that depending on the starting point used in the identification algorithm, multiple solutions for the values of the four viscoelastic parameters (E, c_1, ν, η) have been obtained. The quality of this estimation is discussed using an identifiability analysis. In this aim, an identifiability index (I-index) is used to quantify the richness of the nanoindentation data taken into account in the cost function (Richard et al., 2013). It is also used to define the more adequate experimental procedure and define what would be the experiment(s) to add to a single triangular test in order to assess a unique solution. The identifiability analysis is first performed considering a single nanoindentation triangular test. The effect of nanoindentation depth rate using triangular, trapezoidal, exponential, sinusoidal loading and indenter tip angle is then investigated. The comparison between the I-index results and the dissipation (loss factor) is performed. Finally, the combinations of several nanoindentation triangular tests and indenter tip angles are carried out. A dual nanoindentation technique is shown to yield a unique solution for the inverse problem. To this end, two numerical nanoindentation triangular tests are carried out at a constant depth rate using equivalent cone apex angles of cube corner (42.28°) and Berkovich (70.3°) indenter tips to obtain pseudo-experimental data. The identifiability results for this technique show that a unique solution, which is robust with respect to the noise, can be obtained. However, a poor agreement is found when this solution is compared to the one obtained experimentally. Supported by residual imprint observed on the surface of the sample, plasticity seems to be the cause of this gap. Indeed, a visco-elastic plastic (VEP) model is finally used to describe the material behavior. This VEP model allows a much better agreement between experiment and simulation even if the combination of its five obtained parameters resulting from the updating process is not unique. Finally, it is shown that knowing the yield strength and Poisson's ratio of the material, the identification of the three other parameters is robust, i.e plasticity knowledge helps to identify visco-elastic parameters. These results are supported by a validation performed with tensile response of the material.

2. Material and methods

2.1. Material and viscoelastic law

In this study, a copolymer PP specimen with dimensions of about $10 \times 10 \times 0.5\ \text{mm}^3$ produced by the Goodfellow company has been used (PP301440). An isotropic linear viscoelastic law with constant Poisson's ratio ν is chosen to model the behavior of this material. The Helmholtz free energy ψ (Lemaitre and Chaboche, 1994) can be written as:

$$\psi = \frac{1}{2\rho}(\boldsymbol{\varepsilon}^e : \mathbf{C} : \boldsymbol{\varepsilon}^e + \boldsymbol{\alpha}^{an} : \mathbf{C}^{an} : \boldsymbol{\alpha}^{an}) \tag{1}$$

where $\boldsymbol{\varepsilon}^e$ is the elastic strains tensor, $\boldsymbol{\alpha}^{an}$ is the internal variables tensor representing the anelastic phenomena, ρ is the density, $\mathbf{C}(E, \nu)$ and $\mathbf{C}^{an}(c_1, \nu)$ are the elastic and anelastic fourth-order stiffness tensors. E and c_1 are the instantaneous modulus, and the anelastic modulus, respectively; the symbol ":" stands for the tensor inner product. The state laws derive from this energy:

$$\boldsymbol{\sigma} = \rho \frac{\partial \psi}{\partial \boldsymbol{\varepsilon}^e} \quad \text{and} \quad \mathbf{X}^{an} = \rho \frac{\partial \psi}{\partial \boldsymbol{\alpha}^{an}} \tag{2}$$

where $\boldsymbol{\sigma}$ is the Cauchy stress tensor and $\mathbf{X}^{an}$ is the anelastic stress tensor.

The dissipation potential Ω is defined as:

$$\Omega = \frac{E}{2\eta}(\boldsymbol{\sigma} - \mathbf{X}^{an}) : \mathbf{S} : (\boldsymbol{\sigma} - \mathbf{X}^{an}) \tag{3}$$

where η is the viscosity coefficient and $\mathbf{S}$ the elastic compliance (fourth-order) tensor such as $\mathbf{S} : \mathbf{C} = \mathbf{I}$ (identity tensor). The derivatives of this potential Ω give the internal variables evolutions:

$$\dot{\boldsymbol{\varepsilon}}^{an} = \frac{\partial \Omega}{\partial \boldsymbol{\sigma}} \quad \text{and} \quad \dot{\boldsymbol{\alpha}}^{an} = -\frac{\partial \Omega}{\partial \mathbf{X}^{an}} \tag{4}$$

where $\boldsymbol{\varepsilon}^{an}$ is the anelastic strain which is defined as the difference between the total $\boldsymbol{\varepsilon}$ and elastic $\boldsymbol{\varepsilon}^e$ strains.

$$\boldsymbol{\varepsilon}^{an} = \boldsymbol{\varepsilon} - \boldsymbol{\varepsilon}^e \tag{5}$$

This linear viscoelastic behavior law with constant Poisson's ratio is controlled by four material parameters, which define the parameter set $\boldsymbol{\theta} = (\theta_1, \theta_2, \theta_3, \theta_4) = (E, c_1, \nu, \eta)$.

From a rheological point of view, the chosen behavior is, for elastic contribution, a linear spring whose stiffness is given by the Young's modulus E and Poisson's ratio ν, and for anelastic contribution (delayed elasticity), a classical Kelvin-Voigt model which consists of a linear viscous damper of viscosity η and a linear spring of stiffness c_1 with internal stress X^{an} associated in parallel. One assumes herein a constant Poisson's ratio, so that $E/G = c_1/G_1 = \eta/\eta_G = 2(1+\nu)$ and $E/K = c_1/K_1 = \eta/\eta_K = 3(1-2\nu)$ (Fig. 1).

2.2. Numerical model of the nanoindentation tests

In this paper, a parametric finite element model is built using the ANSYS software, (Ansys 16.0, 2016) (Fig. 1). This 2D-axisymetric model allows the simulation of the nanoindentation test of a viscoelastic material through the ANSYS viscoelastic law. Five conical indenter tips are used, with equivalent half angles equal to 42.28°, 57°, 60°, 65 and 70.3° half angle and are assumed to be rigid. The indenter with 70.3° corresponds to the axisymmetric equivalent cone Berkovich indenter tip used experimentally (Chen et al., 2007; Fischer-Cripps, 2011). The Coulomb's friction law is used between contact surfaces and the friction coefficient has been fixed to 0.2. Note that for this indenter geometry the contact friction coefficient does not have any significant effect on the numerical results (Bucaille et al., 2003). Linear quadrangular elements with 4 nodes (Q4 PLANE182) are used. The size of the modeled sample is 60 times greater than the maximum nanoindentation depth h_{max} in order to obtain realistic boundary conditions. The mesh size in the area right below the indenter is made finer than in the rest of the sample over a length 8 times greater than the h_{max}, which makes possible to model the contact and to increase the precision on the result of the simulation. The mesh is progressively coarser when moving away from the indented area, making it possible to reduce the number of elements and thus reduce the computation time down to 30 minutes (on the sequential CPU mode, 4 processors, 2.5 GHz). The model has about 20,000 finite elements. The nodes belonging to the lower surface of the part of the modeled sample are clamped. For the convergence study, several simulations with refined meshes and time increments are performed with all indenter tips. It is found that from 6 elements below the cube corner indenter (48.28°), 9 elements for the indenters 57°, 60°, and 10 elements for the indenter 65° and the Berkovich indenter (70.3°) at h_{max}, the mesh size has no influence on the obtained results. The nanoindentation test is simulated by two subsequent parts: loading and unloading. During the loading part, the indenter tip penetrates the specimen up to h_{max} and during the unloading part, the indenter returns to the initial position. In each simulation, 1 to 5 iterations are required at each nanoindentation depth increment to reach an equilibrium configuration. At h_{max}, about nine elements are in contact with the indenter tip.

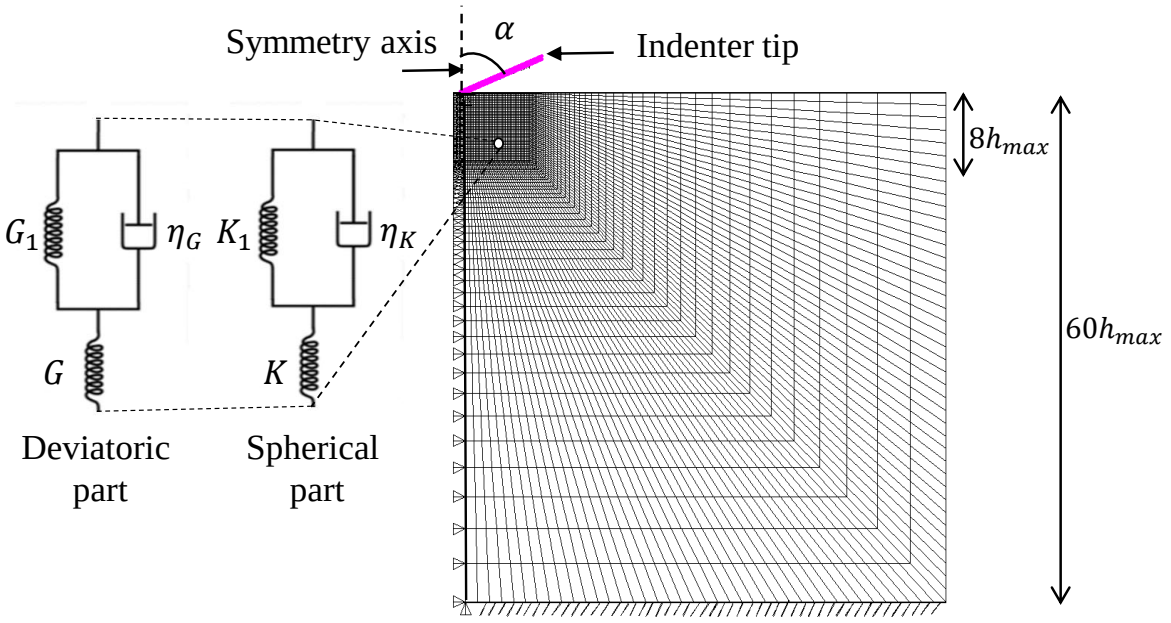

Fig. 1. 2D-axisymmetric model of the nanoindentation test and the rheological model decomposed into: a deviatoric and a spherical part ($E/G = c_1/G_1 = \eta/\eta_G = 2(1+v)$) and ($E/K = c_1/K_1 = \eta/\eta_K = 3(1-2v)$).

2.3. Experimental test

A nanoindentation experimental test was performed at room temperature and relative humidity using an Ultra-Nanoindenter (UNHT) with a Berkovich indenter tip. This device allows to impose a force up to 50 mN ($\pm$0,1 μN) and a displacement up to 40 μm ($\pm$0,1 nm). The test has been carried out in displacement-controlled mode to a maximum value of $h_{max} \approx 550$ nm. Repeating the same experiment 5 times, a standard deviation of 6μN is observed experimentally at h_{max}. It consists of a load-unload cycle. Once the contact established, the indenter penetrates the sample at a quasi-constant nanoindentation depth rate $\dot{h} = 1000$ nm/min until the maximum displacement h_{max}. Then during the unloading phase the indenter is removed at the same rate until $h = 0$. The force $P_{exp}(t)$ and displacement $h_{exp}(t)$ are recorded during loading and unloading segments for a time t_{max}.

2.4. Numerical tests

In order to numerically investigate the parameters identifiability with different loading types and determine the better identification procedure, several nanoindentation tests at a depth of $h_{max} = 500$ nm and time t_{max} are numerically carried out at eight nanoindentation depth rates $\dot{h} = 50$, 100, 500, 1000, 2500, 5000, 10000 and 20000 nm/min for triangular and trapezoidal loading, and eight strain rates ($\dot{h}/h = 0.0104$, 0.0207, 0.1036, 0.2072, 0.5179, 1.0359, 2.0722 and 4.1458 s^{-1}) for the exponential loading. Normalized time-displacement curves are given in Fig. 2.

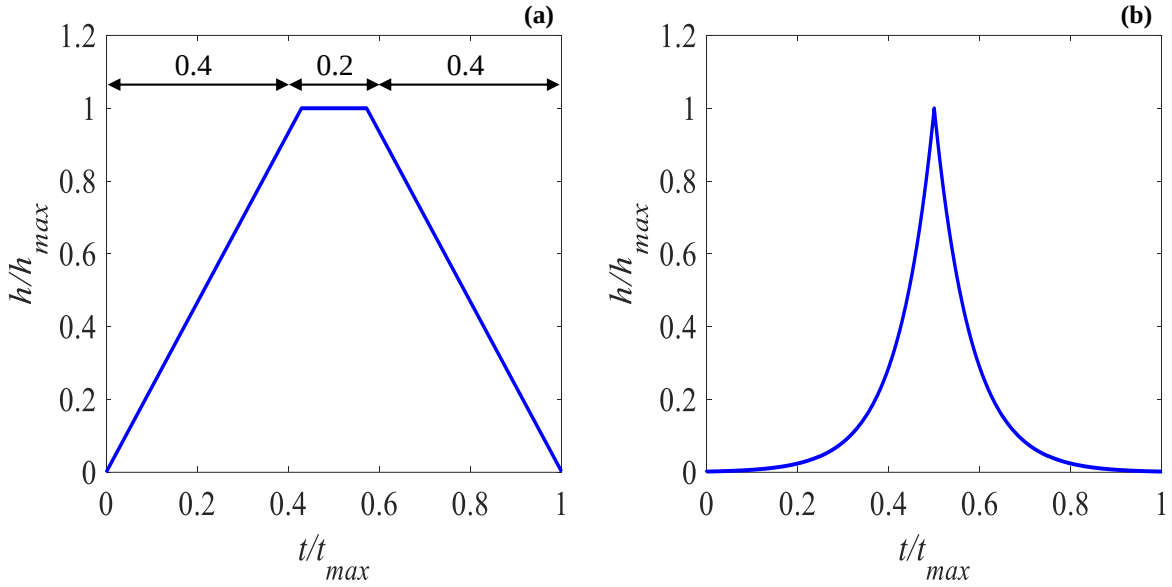

Fig. 2. Normalized time-displacement curves, (a) trapezoidal loading. (b) exponential loading.

Other nanoindentation tests at a depth of $h_{max} = 500$ nm and maximum load of $P_{max} = 0.6$ mN are numerically carried out in force-controlled mode with eight nanoindentation depth rates (60, 120, 600, 1200, 3000, 6000, 12000 and 24000 μN/min) for triangular loading (Fig. 3a). A monotonic loading test is then performed with superimposed sinusoidal loading to a maximum depth of $h_{max} = 510$ nm over a loading time of 30 s and frequency of 4 Hz (Fig. 3b).

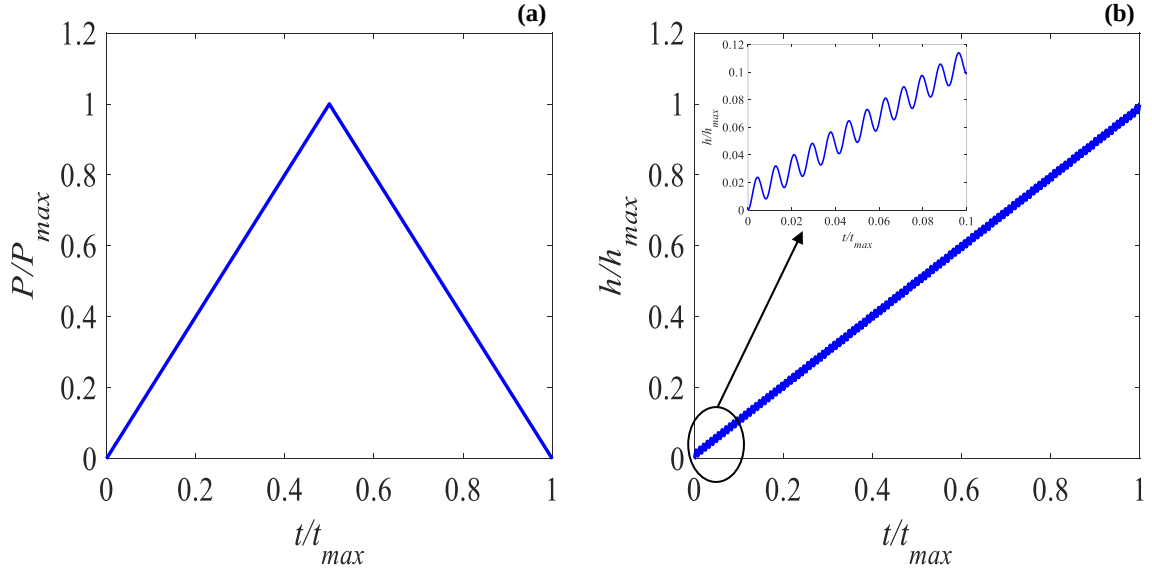

Fig. 3. Normalized time-force curves, (a) triangular loading. Normalized time-displacement (b) sinusoidal loading.

In the following, the computer-generated load-displacement curves obtained from these different conditions will be referred to as pseudo-experimental data.

2.5. Inverse method for the material parameters estimation

The updating process of the numerical model based on the experimental (or pseudo-experimental) data allows to estimate one or more parameters values $\widehat{\boldsymbol{\theta}}$ which minimize the difference between the force $P(t;\boldsymbol{\theta})$ resulting from the finite element simulation and the experimental data $P^{exp}(t)$. The inverse problem is recast as the minimization problem of an objective function ω, which quantifies the difference between the numerical model and the experiment:

$$\widehat{\boldsymbol{\theta}} = \underset{\boldsymbol{\theta}}{\operatorname{argmin}}\ \omega\ [P(t;\boldsymbol{\theta}), P^{exp}(t)] \tag{6}$$

The objective function ω is minimized by a local numerical optimization technique based on the Levenberg-Marquardt algorithm (Levenberg, 1944; Marquardt, 1963) implemented in MIC2M software (F. Richard, 2000). A starting point is required in this algorithm. The influence of this point will be investigated. The objective function is defined in displacement-controlled mode as (Qasmi et al., 2004):

$$\omega(\boldsymbol{\theta}) = \frac{1}{2T}\sum_{k=1}^{T}\left[\frac{P_k(\boldsymbol{\theta}) - P_k^{exp}}{P_{max}^{exp}}\right]^2 \tag{7}$$

$T = 1000$ is the number of data points for each nanoindentation test, i.e. number of measured force values $P_k(\boldsymbol{\theta}) = P(t_k;\boldsymbol{\theta})$ and $P_k^{exp} = P^{exp}(t_k)$, and P_{max}^{exp} is the maximum of the experimental nanoindentation force. T is sufficiently large so that it does not influence the reported results.

The uncertainty $\Delta\theta_j$ on the estimated value of θ_j after the updating process can be obtained from the following equation in $\theta_j = \hat{\theta}_j$:

$$\frac{\Delta\theta_j}{\theta_j} = \sqrt{2\omega[\bar{\mathbf{H}}^{-1}]_{jj}} \tag{8}$$

where $\bar{\mathbf{H}}$ is a dimensionless pseudo-hessian matrix computed by forward finite difference method (Pac et al., 2014; Richard et al., 2013). The components of $\bar{\mathbf{H}}$ are given as:

$$\bar{H}_{ij} = \frac{1}{T}\frac{\theta_i\theta_j}{P_{max}^2}\sum_{k=1}^{T}\frac{\partial P_k(\boldsymbol{\theta})}{\partial\theta_i}\frac{\partial P_k(\boldsymbol{\theta})}{\partial\theta_j} \qquad i,j = 1,\dots,4 \tag{9}$$

where P_{max} is the maximum of the numerical nanoindentation force.

Note that if the test is force-controlled, the objective function is formulated using the displacement response $h(t;\boldsymbol{\theta})$, instead of $P(t;\boldsymbol{\theta})$.

When a combination of several nanoindentation tests n is used in the updating process, the total objective function is given by the sum of the objective functions of all tests.

$$\omega(\boldsymbol{\theta}) = \sum_{e=1}^{n}\left[\frac{1}{2T}\sum_{k=1}^{T}\left(\frac{P_k^{(e)}(\boldsymbol{\theta}) - P_k^{exp^{(e)}}}{P_{max}^{exp^{(e)}}}\right)^2\right] \tag{10}$$

The uncertainty becomes:

$$\frac{\Delta\theta_j}{\theta_j} = \sqrt{\frac{2}{n}\omega[\bar{\mathbf{H}}^{-1}]_{jj}} \tag{11}$$

and the pseudo-hessian matrix $\bar{\mathbf{H}}$ is calculated from the following equation:

$$\bar{H}_{ij} = \sum_{e=1}^{n}\left[\frac{1}{T}\frac{\theta_i\theta_j}{\left(P_{max}^{(e)}\right)^2}\sum_{k=1}^{T}\frac{\partial P_k^{(e)}(\boldsymbol{\theta})}{\partial\theta_i}\frac{\partial P_k^{(e)}(\boldsymbol{\theta})}{\partial\theta_j}\right] \quad i,j = 1,\dots,4 \tag{12}$$

2.6. Parametric identifiability

The sensitivity analysis is performed to evaluate how, and to which extent, variations of the model input data influence the output data. In this analysis, the value of each parameter is changed by 0.1% with respect to its initial value in the study. Using a finite difference scheme, the sensitivity vectors are given by (for a single test):

$$S_{kj} = \frac{\theta_j}{P_{max}}\frac{\partial P_k}{\partial\theta_j} \tag{13}$$

The sensitivity of the nanoindentation force to the parameter θ_j can be computed as:

$$\delta_j = \frac{\theta_j}{P_{max}}\sqrt{\frac{1}{T}\sum_{k=1}^{T}\left(\frac{\partial P_k}{\partial\theta_j}\right)^2} \tag{14}$$

A parametric identifiability analysis is used to quantify the reliability of the estimated parameters. The completeness of data contained in the nanoindentation force is quantified by an I-index (Richard et al., 2013). This index appears to be convenient to explore and investigate what are the optimal loading conditions to determine the four parameters of the material constitutive law. The analysis can be done before and after the updating process and therefore does not necessarily require the experimental measurements (only pseudo-experimental loading). The I-index is a measure of the conditioning of the inverse problem and is defined as (Pac et al., 2014):

$$I = \log_{10}\left(\frac{\lambda_{max}}{\lambda_{min}}\right) > 0 \quad (15)$$

where λ_{max} and λ_{min} are the maximum and minimum eigenvalue of the matrix $\bar{\mathbf{H}}$ at the considered calculation point $\boldsymbol{\theta}$, respectively. The I-index is calculated as function of the sensitivity of parameters taken into account in the combination. In the case of combination of nanoindentation tests, I_{min} and I_{max} are the minimum and maximum of the I-index for the better and worse combination, respectively.

The lower the I-index, the better conditioned is the matrix, which means its inverse can be calculated with great accuracy. At the opposite, if the I-index is large, the matrix is considered as ill-conditioned. Some I-index values defining practical limits can be found in the literature (Gujarati, D.N, 1988). For a chosen set of parameters $\boldsymbol{\theta}$ and loading type, this I-index is calculated for the 11 parameter combinations (6 couples, 4 triplets and 1 quadruplet) and for various time subsets (load-unload, load only, unload only). This procedure allows to distinguish the potentially identifiable combinations ($I \leq 2$) of material parameters from those which are not ($I > 3$).

3. Results and discussions

In this section, the results of the updating process of the FEM are presented in terms of estimated values of the parameters and associated uncertainties. The uniqueness/non-uniqueness of the viscoelastic properties of PP obtained from a single nanoindentation experimental triangular load-unload test is studied. The identifiability analysis is numerically performed using several loading types (trapezoidal, exponential, sinusoidal) and angles apex in order to propose an identification procedure for the four viscoelastic material parameters (E, c_1, ν, η). A link between the identifiability results and the dissipated energy is shown. The addition of the plasticity in behavior law is carried out for a complete description of the material behavior.

3.1. Non-uniqueness of the solutions

3.1.1. Updating process from experimental data

Experimental data from the nanoindentation test realized on PP at 1000 nm/min using the triangular loading are used in equation (Eq.6). Three starting points $\boldsymbol{\theta}^{(01)}$, $\boldsymbol{\theta}^{(02)}$ and $\boldsymbol{\theta}^{(03)}$ are chosen to initialize the minimization algorithm (Table 1) and solve the minimization problem. The evolution of the four parameters during the minimization process are shown in Fig. 4. The parameters E, c_1 and η tend towards the same values whatever the starting point with acceptable uncertainties (about 15% for the viscosity η). However the obtained values for Poisson's ratio ν are multiple with an enormous uncertainty (about 140%). The value of the objective function ω is almost identical for all three cases and remains very low. Therefore there is non-uniqueness of the solution of the inverse problem. Fig. 5 illustrates that the obtained solutions generate almost the same *P-h* curve as the one obtained experimentally.

Table 1. Estimated parameters set $\widehat{\boldsymbol{\theta}}$ (Eq. 6) using three starting points and uncertainties (Eq.8).

		Parameter	Starting value	Estimated value	Uncertainty
	j	θ_j	$\theta_j^{(0)}$	$\hat{\theta}_j$	$\Delta\theta_j/\theta_j$ (%)
Starting point 1: $\boldsymbol{\theta}^{(01)}$	1	E (GPa)	1.50	1.63	7.0
	2	c_1 (GPa)	12.25	1.05	6.0
	3	ν	0.4	0.13	90
	4	η (GPa. s)	65	18.56	15
Objective function $\omega^{(1)}$			4.59×10^{-2}	1.24×10^{-5}	
Starting point 2: $\boldsymbol{\theta}^{(02)}$	1	E (GPa)	1.40	1.63	6.0
	2	c_1 (GPa)	8.0	1.05	6.0
	3	ν	0.3	0.03	137
	4	η (GPa. s)	45	18.48	15
Objective function $\omega^{(2)}$			2.18×10^{-2}	1.24×10^{-5}	
Starting point 3: $\boldsymbol{\theta}^{(03)}$	1	E (GPa)	1.20	1.63	7.0
	2	c_1 (GPa)	4.0	1.06	6.0
	3	ν	0.2	0.03	138
	4	η (GPa. s)	30	18.50	15
Objective function $\omega^{(3)}$			5.18×10^{-3}	1.24×10^{-5}	

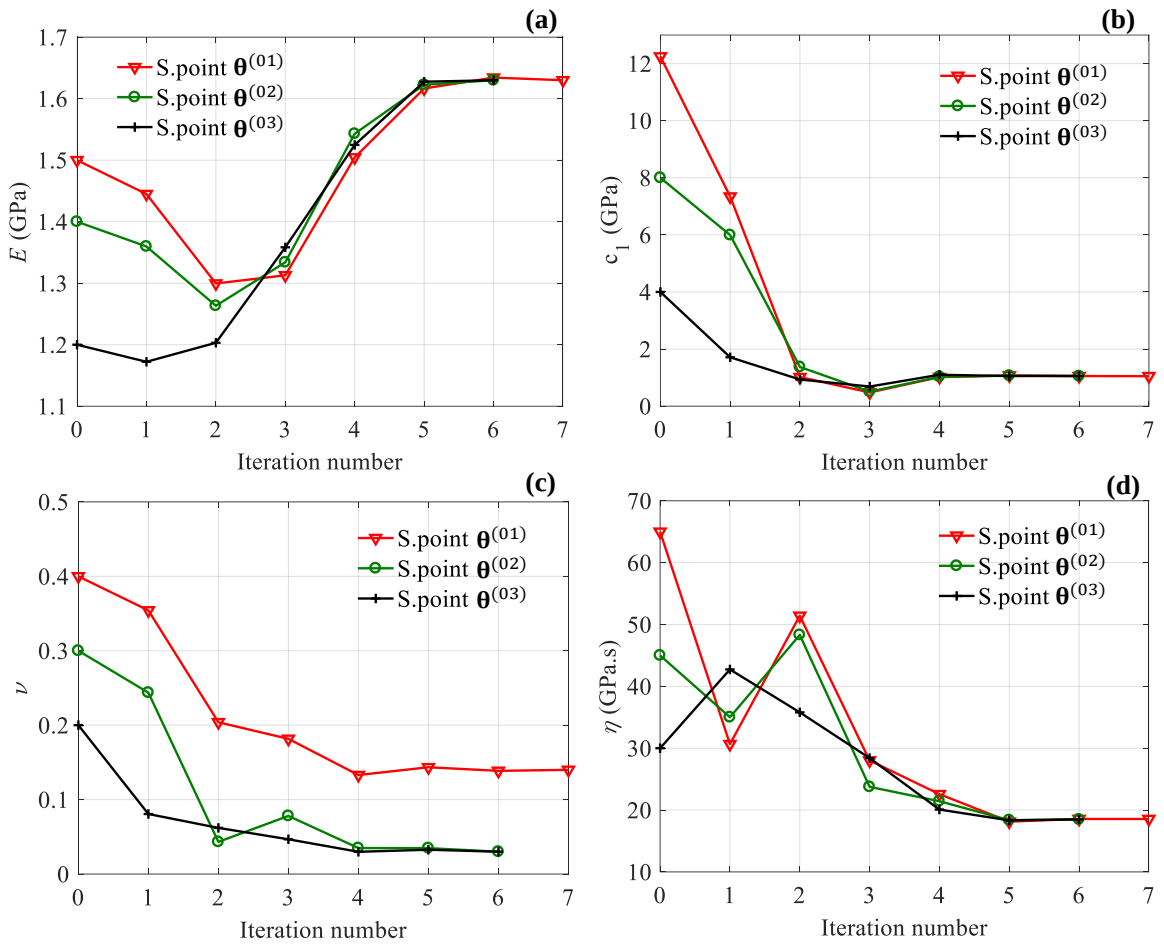

Fig. 4. Evolution of the four parameters (E, c_1, ν, η) during the updating process using three starting points $\boldsymbol{\theta}^{(01)}$, $\boldsymbol{\theta}^{(02)}$ and $\boldsymbol{\theta}^{(03)}$.

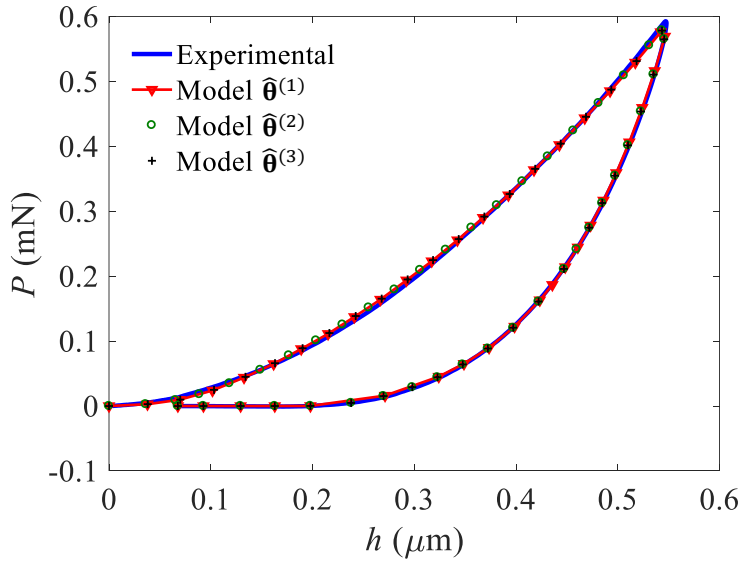

Fig. 5. Experimental ($\dot{h} = 1000$ nm/min) and simulated nanoindentation curves for the three solutions $\widehat{\boldsymbol{\theta}}^{(1)} = (E = 1.63$ GPa, $c_1 = 1.05$ GPa, $\nu = 0.13$, $\eta = 18.56$ GPa.s), $\widehat{\boldsymbol{\theta}}^{(2)} = (E = 1.63$ GPa, $c_1 = 1.05$ GPa, $\nu = 0.03$, $\eta = 18.48$ GPa.s) and $\widehat{\boldsymbol{\theta}}^{(3)} = (E = 1.63$ GPa, $c_1 = 1.06$ GPa, $\nu = 0.03$, $\eta = 18.50$ GPa.s).

Furthermore, the Poisson's ratio is badly estimated comparing the obtained value with those given in the literature (ν~0.3 to 0.42) (Gao and Mäder, 2002; Jakes et al., 2008). Updating processes can also be performed by imposing one of the four parameters. Two particular cases are considered. In the first case A, the Young's modulus E is set to 1.50 GPa and the three parameters ν, c_1 and η are estimated (starting point: $\boldsymbol{\theta}^{(04)} = (E = 1.50\ \text{GPa (imposed)}, c_1 = 12.25\ \text{GPa}, \nu = 0.4,\ \eta = 65\ \text{GPa.s})$). In the second case B, the value of the Poisson's ratio ν is set to 0.4 and E, c_1 and η are estimated (starting point: $\boldsymbol{\theta}^{(05)} = (E = 1.50\ \text{GPa}, c_1 = 12.25\ \text{GPa}, \nu = 0.4\ \text{(imposed)},\ \eta = 65\ \text{GPa.s})$). Fig. 6 shows the evolution of the four parameters during the minimization process. The obtained values are multiple except for the parameter c_1. The parameters estimated resulting from the updating process are presented in Table 2. It can be noted that imposing a parameter increases considerably the uncertainties even on E and c_1.The objective function values are not identical for the two solutions but they are the same order in magnitude. The five solutions $\widehat{\boldsymbol{\theta}}^{(1)}$, $\widehat{\boldsymbol{\theta}}^{(2)}$, $\widehat{\boldsymbol{\theta}}^{(3)}$, $\widehat{\boldsymbol{\theta}}^{(4)}$ and $\widehat{\boldsymbol{\theta}}^{(5)}$ are summarized in Table 3. All of the *P-h* curves are in good agreement with the experimental data (Fig. 7). It is interesting to note that Young's modulus $E = 1.65$ GPa obtained from the nanoindentation experimental test at 1000 nm/min using the Oliver-Pharr method (Oliver and Pharr, 1992) using a Poisson's ratio $\nu = 0.4$ is approximately 12% higher than this estimated by FEMU (case B).

Table 2. Estimated parameters for the two particular cases A and B.

		Parameter	Starting value	Estimated value	Uncertainty
	j	θ_j	$\theta_j^{(0)}$	$\hat{\theta}_j$	$\Delta\theta_j/\theta_j$ (%)
Starting point 4: $\boldsymbol{\theta}^{(04)}$ (Case A)	1	E (GPa)	1.50 (imposed)	1.50 (imposed)	10
	2	c_1 (GPa)	12.25	0.96	24
	3	ν	0.4	0.02	291
	4	η (GPa.s)	65	22.87	29
Objective function $\omega^{(4)}$			4.59×10^{-2}	3.27×10^{-5}	
Starting point 5: $\boldsymbol{\theta}^{(05)}$ (Case B)	1	E (GPa)	1.50	1.47	44
	2	c_1 (GPa)	12.25	0.94	48
	3	ν	0.4 (imposed)	0.4 (imposed)	145
	4	η (GPa.s)	65	17.08	41
Objective function $\omega^{(5)}$			4.59×10^{-2}	1.31×10^{-5}	

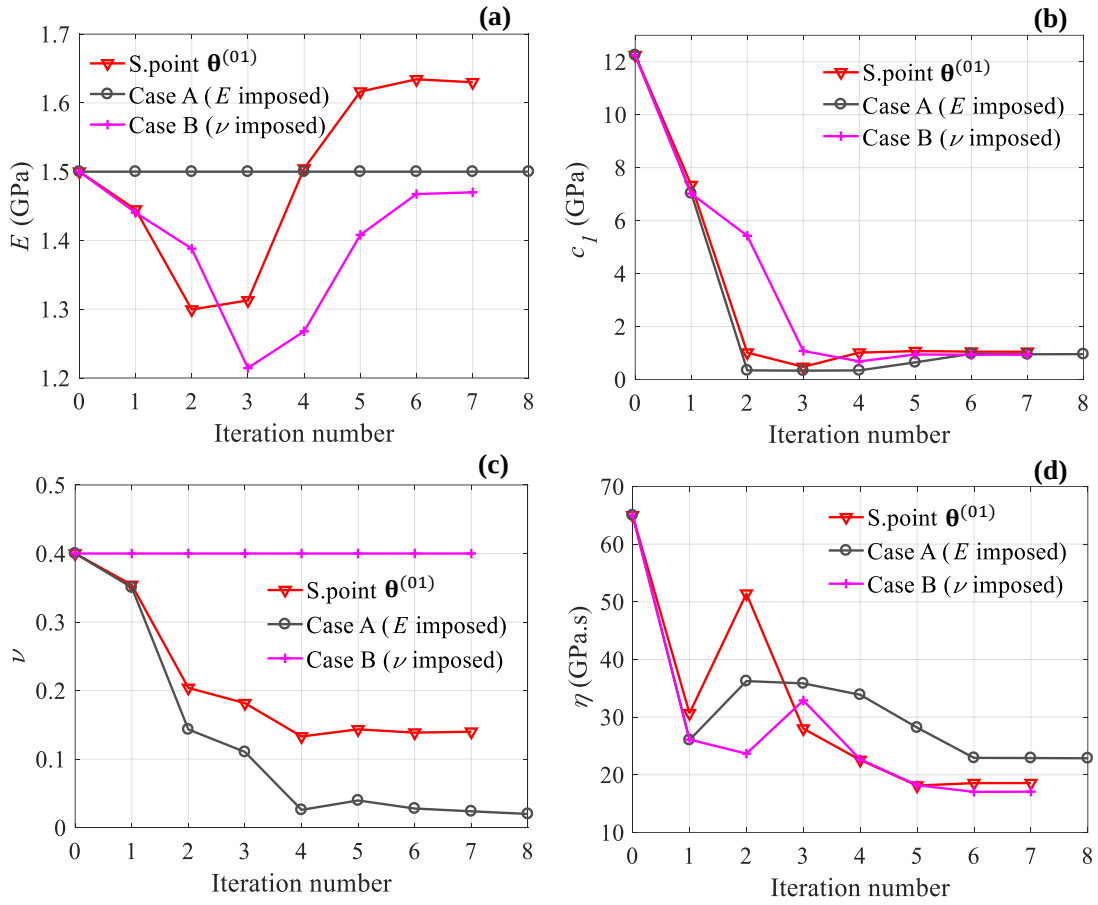

Fig. 6. Evolution of the four parameters (E, c_1, ν, η) during the updating process for the two particular cases A and B. Comparison with a case with 4 free parameters for the starting point ($\boldsymbol{\theta}^{(01)} = E =$ 1.5 GPa, $c_1 = 12.25$ GPa, $\nu = 0.4$, $\eta = 65$ GPa.s).

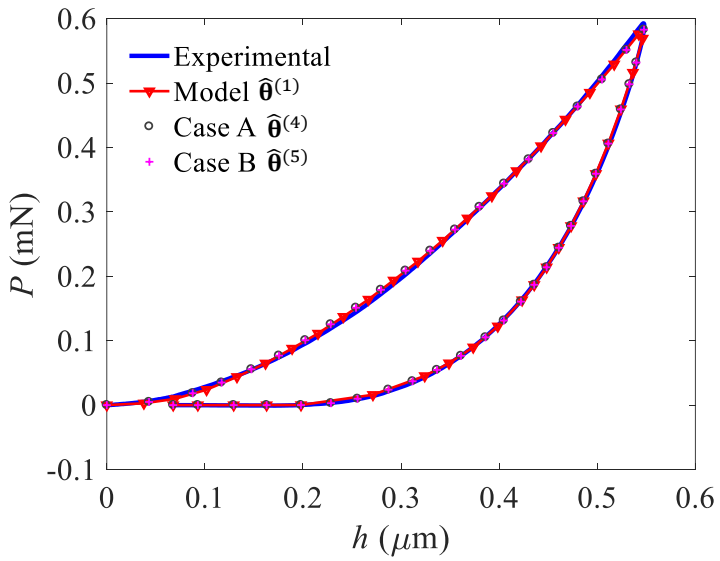

Fig. 7. Experimental ($\dot{h} = 1000$ nm/min) and simulated nanoindentation curves for the three solutions $\widehat{\boldsymbol{\theta}}^{(1)} = (E = 1.63$ GPa, $c_1 = 1.05$ GPa, $\nu = 0.13$, $\eta = 18.56$ GPa.s), $\widehat{\boldsymbol{\theta}}^{(4)} = (E = 1.50$ GPa, $c_1 = 0.96$ GPa, $\nu = 0.02$, $\eta = 22.87$ GPa.s) and $\widehat{\boldsymbol{\theta}}^{(5)} = (E = 1.47$ GPa, $c_1 = 0.94$ GPa, $\nu = 0.4$, $\eta = 17.08$ GPa.s).

Table 3. Five solutions of the inverse problem.

j	1	2	3	4	
Solution	E (GPa)	c_1 (GPa)	ν	η (GPa. s)	ω
$\widehat{\boldsymbol{\theta}}^{(1)}$	1.63	1.05	0.13	18.56	1.24×10^{-5}
$\widehat{\boldsymbol{\theta}}^{(2)}$	1.63	1.05	0.03	18.48	1.24×10^{-5}
$\widehat{\boldsymbol{\theta}}^{(3)}$	1.63	1.06	0.03	18.50	1.24×10^{-5}
$\widehat{\boldsymbol{\theta}}^{(4)}$	1.50 (imposed)	0.96	0.02	22.87	3.27×10^{-5}
$\widehat{\boldsymbol{\theta}}^{(5)}$	1.47	0.94	0.4 (imposed)	17.08	1.31×10^{-5}

3.1.2. Sensitivity analysis

To probe the uniqueness of a solution resulting from an updating process may appear to be very time consuming. In fact, an updating process for four parameters requires about 40 FEM computations for each starting point and for each experimental loading. Another way is to investigate, a priori, the identifiability of the parameters. In this way, it is needed to estimate the sensitivity of the nanoindentation force to the material parameters. A sensitivity analysis is performed for the five solutions $\widehat{\boldsymbol{\theta}}^{(1)}$, $\widehat{\boldsymbol{\theta}}^{(2)}$, $\widehat{\boldsymbol{\theta}}^{(3)}$, $\widehat{\boldsymbol{\theta}}^{(4)}$ and $\widehat{\boldsymbol{\theta}}^{(5)}$ (2.5 hours for each solution) using the numerical nanoindentation triangular test realized at 1000 nm/min in displacement-controlled mode. The norm of sensitivity vectors calculated using equation (Eq.14) are displayed in Fig. 8. The Young's modulus E is the most sensitive parameter, which means that it is the most influential to the nanoindentation curve. The sensitivities appear to be well balanced for each solution. An exception can be noted for the Poisson's ratio. In fact, there is a lack of sensitivity to ν for the solutions $\widehat{\boldsymbol{\theta}}^{(1)}$, $\widehat{\boldsymbol{\theta}}^{(2)}$, $\widehat{\boldsymbol{\theta}}^{(3)}$ and $\widehat{\boldsymbol{\theta}}^{(4)}$ where the sensitivity to this coefficient is close to zero (Fig. 8). It is noted that the sensitivity of the nanoindentation force to the friction ratio can be neglected.

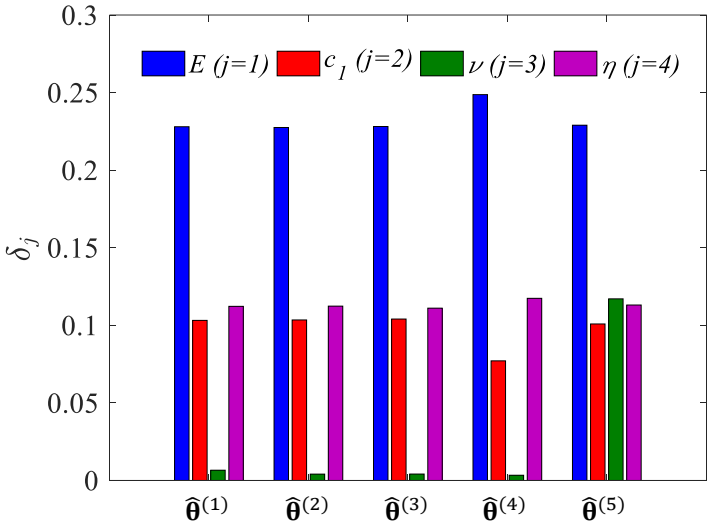

Fig. 8. Sensitivity of the nanoindentation force P to θ_j for the five solutions $\widehat{\boldsymbol{\theta}}^{(1)}$, $\widehat{\boldsymbol{\theta}}^{(2)}$, $\widehat{\boldsymbol{\theta}}^{(3)}$, $\widehat{\boldsymbol{\theta}}^{(4)}$ and $\widehat{\boldsymbol{\theta}}^{(5)}$ (Table 3) using triangular test at 1000 nm/min.

The sensitivity vectors of the nanoindentation force have thus been calculated using equation (Eq.13) for the solution $\widehat{\boldsymbol{\theta}}^{(5)}$. Fig. 9a shows that these vectors are very similar (up to a multiplicative factor) during the loading phase. The identification of these four parameters from the sole loading phase is thus expected to be very difficult. Focusing on the sensitivity to E we note that during the unloading part the proportionality with c_1 and η is lost. It seems to indicate that the unloading segment is more suitable to distinguish solution parameters and so to identify them. It also appears that the sensitivity vectors to E and ν are almost collinear during the loading segment (OA) in (Fig. 9b), thus their identification using a single nanoindentation loading data is impossible. This is understood as a consequence of the sensitivity of the Boussinesq's problem to the sole $E/(1-\nu^2)$ parameter (Boussinesq, 1885).

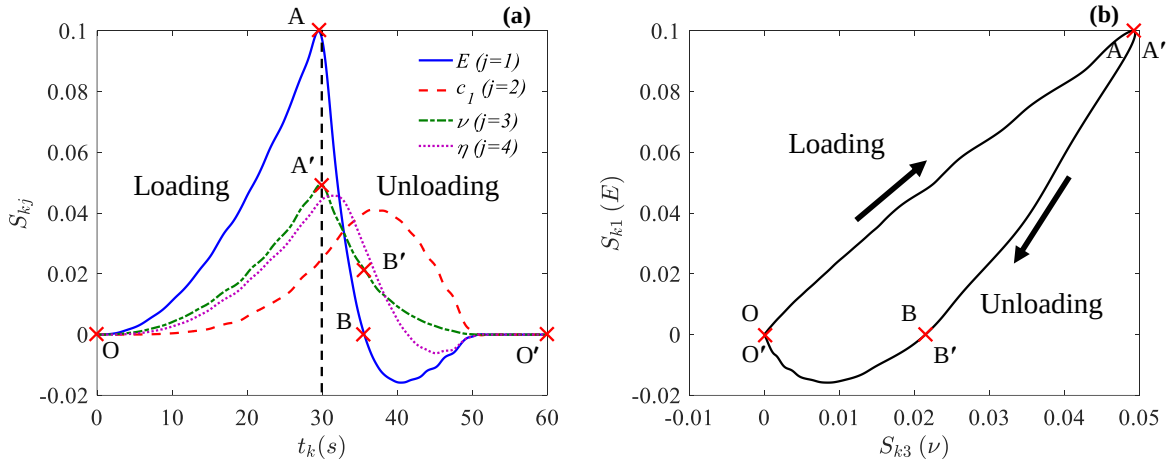

Fig. 9. (a) Sensitivity vectors of the nanoindentation force to the material parameters θ_j during loading and unloading. (b) collinearity between sensitivity vectors S_{k1} and S_{k3} (sensitivities to E and ν, respectively).

3.1.3. A posteriori identifiability analysis

To quantify the completeness of the data used in the updating process, the I-index is determined from equation (Eq.15) using the solution $\widehat{\boldsymbol{\theta}}^{(5)}$ with the numerical nanoindentation triangular test realized at 1000 nm/min for the 11 possible combinations of parameters as a function of the considered data subsets (load-unload, load and unload) and summarized in Table 4. The identification of all combinations of two parameters is possible from load-unload test and only unloading segment. It seems possible to identify three parameters (E, c_1, η) when the Poisson's ratio is known. The value of the index $I(E, c_1, \eta)$ is greater than 3 only when the sole loading segment is considered and less than 2 as soon as the unloading phase is taken into account. For this combination of parameters, the identifiability is better if only unload is considered ($I = 1.5$) than if both load and unload are considered ($I = 1.9$). It can be observed that the relevant information is therefore contained in the unloading part, confirming the conclusions drawn from the sensitivity vectors analysis. The I-index is higher than 3 for the combination of four parameters from single nanoindentation load-unload test. The identification of the full set of parameters is considered to be impossible because of the inverse problem is too ill-posed.

Table 4. I-index for all combinations of parameters using triangular test at 1000 nm/min with the solution $\widehat{\boldsymbol{\theta}}^{(5)}$. $I \leq 2$ (green, potentially identifiable), $2 < I \leq 3$ (difficult to identify), $I > 3$ (red, not identifiable).

Combination	Load-unload	Load	Unload
E, c_1	0.8	2.5	0.2
c_1, η	0.8	2.1	0.8
c_1, ν	0.8	2.1	1.0
E, η	1.4	2.8	0.8
E, ν	1.6	3.1	0.9
ν, η	1.9	3.0	1.8
E, c_1, η	1.9	3.5	1.5
c_1, ν, η	2.1	3.2	2.2
E, ν, η	2.5	3.8	2.1
E, c_1, ν	3.0	3.7	2.6
E, c_1, ν, η	3.7	3.9	3.5

3.2. A priori identifiability analysis of experimental approaches based on a single nanoindentation test

In this section, we focus on the possibility to identify the viscoelastic parameters from a single nanoindentation test. The effects of nanoindentation depth rate, loading type (triangular, trapezoidal, exponential and sinusoidal) and the indenter tip angle are investigated.

3.2.1. Effect of the nanoindentation depth rate

The I-index is calculated for the other numerical nanoindentation triangular load-unload tests (50, 100, 500, 2500, 5000, 10000, 20000 nm/min) with the solution $\widehat{\boldsymbol{\theta}}^{(5)}$. Table 5 shows that it is possible to identify three parameters when using a nanoindentation depth rate between 500 and 1000 nm/min ($I \leq 2$).The nanoindentation depth rate does not improve the four material parameter I-index ($I > 3$). It can be concluded that whatever the nanoindentation depth rate, in the considered range the identification of the four material parameter from single nanoindentation triangular test is impossible.

Table 5. I-index for all combinations of parameters for all nanoindentation triangular load-unload tests using the solution $\widehat{\boldsymbol{\theta}}^{(5)}$. $I \leq 2$ (green, potentially identifiable), $2 < I \leq 3$ (difficult to identify), $I > 3$ (red, not identifiable).

Combination	50 nm/min	100 nm/min	500 nm/min	1000 nm/min	2500 nm/min	5000 nm/min	10000 nm/min	20000 nm/min
E, c_1	2.3	1.7	0.6	0.8	1.9	2.8	3.7	4.2
c_1, η	2.2	1.7	0.6	0.8	1.7	2.3	2.3	2.2
c_1, ν	2.7	2.2	1.1	0.8	1.3	2.0	2.8	3.2
E, η	1.8	1.4	1.6	1.4	1.3	1.5	2.0	2.5

E, ν	2.8	2.5	1.6	1.6	2.0	2.4	2.9	3.4
ν, η	1.6	1.1	1.1	1.9	1.3	1.1	1.2	1.6
E, c_1, η	3.3	3.1	1.8	1.9	3.0	3.7	4.0	4.3
c_1, ν, η	3.4	3.3	2.3	2.1	2.5	3.0	3.1	3.3
E, ν, η	3.0	2.9	1.8	2.6	3.7	4.0	4.2	4.3
E, c_1, ν	3.5	3.5	2.9	3.0	3.6	4.0	4.2	4.4
E, c_1, ν, η	3.5	3.5	3.6	3.7	4.0	4.1	4.3	4.4

3.2.2. Effect of the loading type

The identifiability analysis is also performed using the trapezoidal, exponential and sinusoidal numerical tests (Table 6). Three parameters (E, c_1, η) are potentially identifiable ($I \leq 2$) when the Poisson's ratio is known using trapezoidal loading. Comparing the results from single nanoindentation test in terms of I-index, the addition of a plateau just after the loading phase does not appear very helpful. It is observed that the better identifiability of the three parameters (E, c_1, η) is obtained using the exponential loading. Finally, the addition of a sinusoidal signal at the chosen frequency to the triangular loading phase is no more interesting for this material and all combinations of parameters are in the best case difficult to identify.

Table 6. I-index for different loading types ($[I_{min}; I_{max}]$): triangular, trapezoidal, exponential and a sinusoidal loading with max rate (1020 nm/min). $I \leq 2$ (green, potentially identifiable), $2 < I \leq 3$ (difficult to identify), $I > 3$ (red, not identifiable).

Combination	Triangular load-unload	Trapezoidal load-unload	Exponential load-unload	Triangular load	Sinusoidal load
E, c_1	[0.6; 4.2]	[0.6; 4.2]	[0.6; 5.7]	2.5	2.5
c_1, η	[0.6; 2.3]	[0.7; 2.5]	[0.7; 2.6]	2.1	2.1
c_1, ν	[0.8; 3.2]	[0.9; 3.2]	[1.1; 4.6]	2.1	2.1
E, η	[1.3; 2.5]	[1.2; 2.3]	[1.1; 3.8]	2.8	2.7
E, ν	[1.6; 3.4]	[1.6; 3.3]	[1.6; 4.1]	3.1	3.1
ν, η	[1.1; 1.9]	[0.9; 1.9]	[0.7; 2.3]	3.0	2.9
E, c_1, η	[1.8; 4.3]	[2.0; 4.4]	[1.6; 5.7]	3.5	3.4
c_1, ν, η	[2.0; 3.4]	[2.3; 3.6]	[2.1; 4.7]	3.2	3.1
E, ν, η	[1.8; 4.3]	[2.3; 4.4]	[1.8; 4.5]	3.8	3.7
E, c_1, ν	[2.9; 4.4]	[3.1; 4.5]	[2.7; 5.7]	3.7	3.7
E, c_1, ν, η	[3.5; 4.4]	[3.6; 4.5]	[3.7; 5.7]	3.9	3.8

3.2.3. Effect of the indenter tip angle

A study has also been conducted to investigate the influence of the half angle α of the indenter tip on the I-index. Five indenter tips with equivalent half angle of $\alpha = 42.28°$ (cube corner), 57°, 60°, 65° and 70.3° (Berkovich) are considered. The I-index results obtained for a nanoindentation depth rate of 500 nm/min using these indenter tips are given in Table 7.

Comparing the values of the I-index, it is found that the angle of the indenter does not have a great influence on the identifiability. The I-index values are almost the same and the four material parameters are, in the best case difficult to identify.

Table 7. I-index for all combinations of parameters using the nanoindentation load-unload test of 500 nm/min with five indenter angles tips for the solution $\widehat{\boldsymbol{\theta}}^{(5)}$. $I \leq 2$ (green, potentially identifiable), $2 < I \leq 3$ (difficult to identify), $I > 3$ (red, not identifiable).

Combination	Cube corner ($\alpha = 42.28°$)	$\alpha = 57°$	$\alpha = 60°$	$\alpha = 65°$	Berkovich ($\alpha = 70.3°$)
E, c_1	0.5	0.6	0.6	0.6	0.6
c_1, η	0.6	0.6	0.6	0.6	0.6
c_1, ν	1.4	1.1	1.1	1.1	1.1
E, η	1.5	1.6	1.6	1.6	1.6
E, ν	1.8	1.6	1.6	1.6	1.6
ν, η	1.0	1.0	1.0	1.1	1.1
E, c_1, η	1.7	1.8	1.8	1.8	1.8
c_1, ν, η	2.2	2.3	2.3	2.3	2.3
E, ν, η	1.9	1.8	1.8	1.8	1.8
E, c_1, ν	2.7	2.8	2.8	2.8	2.9
E, c_1, ν, η	2.8	3.2	3.1	3.4	3.6

3.2.4. Link between dissipation and identifiability

The loss factor (intrinsic damping) $\tan(\delta)$, which is used to measure a viscoelastic material property in the case of tensile and harmonic loading can be approached for any of the considered loading signals considered herein, by discording any signal harmonic so that:

$$\tan(\delta) = \frac{2\pi f E \eta}{c_1(E + c_1) + (2\pi f)^2 \eta^2} \tag{16}$$

where f is the fundamental frequency. In the case of the nanoindentation test $f = 1/t_{max}$.

The I-index is calculated for the numerical nanoindentation triangular tests with equivalent cube corner and Berkovich indenter tips using displacement-controlled and force-controlled modes to investigate the effect of nanoindentation rate.

Fig. 10 presents the results for three combinations of parameters calculated using the solution $\widehat{\boldsymbol{\theta}}^{(5)}$ with the equivalent cube corner indenter tip. It can be observed that the I-index values of the four parameters fall for the three slowest rates (60, 120 and 600 μN/min) (Fig. 10b). This numerical problem disappears if the Poisson's ratio is known. The better identifiability of the material parameters is obtained with a nanoindentation depth rate between 500 nm/min ($t_{max} = 120\ s$) and 1000 nm/min ($t_{max} = 60\ s$) in displacement-controlled mode and a nanoindentation load rate 600 μN/min ($t_{max} = 120\ s$) and 1200 μN/min ($t_{max} = 60\ s$) in force-controlled mode. It also shows that the I-index is well correlated to the loss factor (Fig.

10). In particular, we note that when the loss factor is maximum, (i.e when the dissipation is maximum) the I-index is minimum, (i.e the identifiability is the maximum).

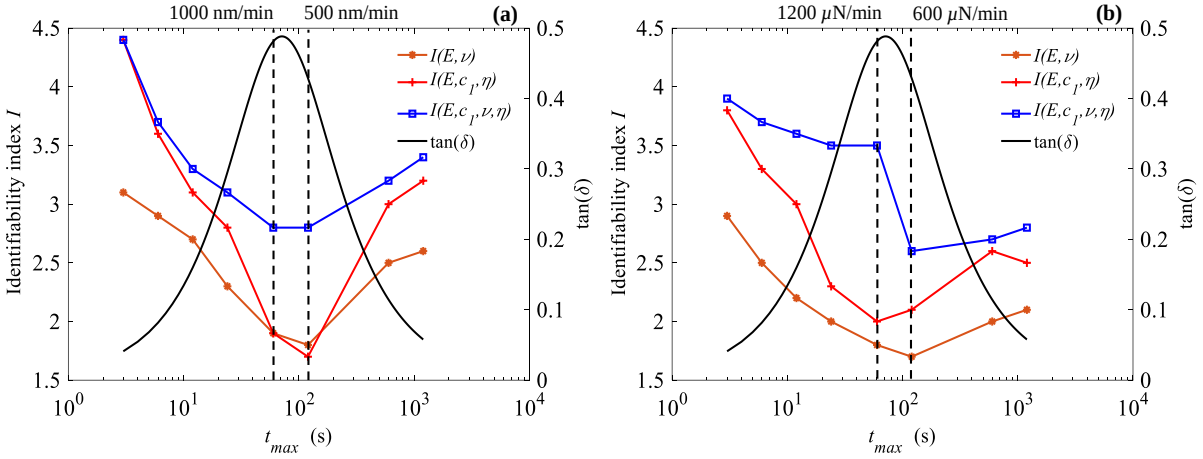

Fig. 10. I-index for the nanoindentation triangular tests and the loss factor using the solution $\widehat{\boldsymbol{\theta}}^{(5)}$ with equivalent cube corner indenter tip, (a) displacement-controlled mode. (b) force-controlled mode.

For the equivalent Berkovich indenter tip (Fig. 11), it can be seen that the better identifiability of the material parameters is obtained with a nanoindentation depth rate between 500 nm/min ($t_{max} = 120\ s$) and 1000 nm/min ($t_{max} = 60\ s$) in displacement-controlled mode and a nanoindentation load rate about 1200 μN/min ($t_{max} = 60\ s$) in force-controlled mode. It also shows that the I-index is well correlated to the loss factor (Fig. 11), similarly to equivalent cube corner indenter tip.

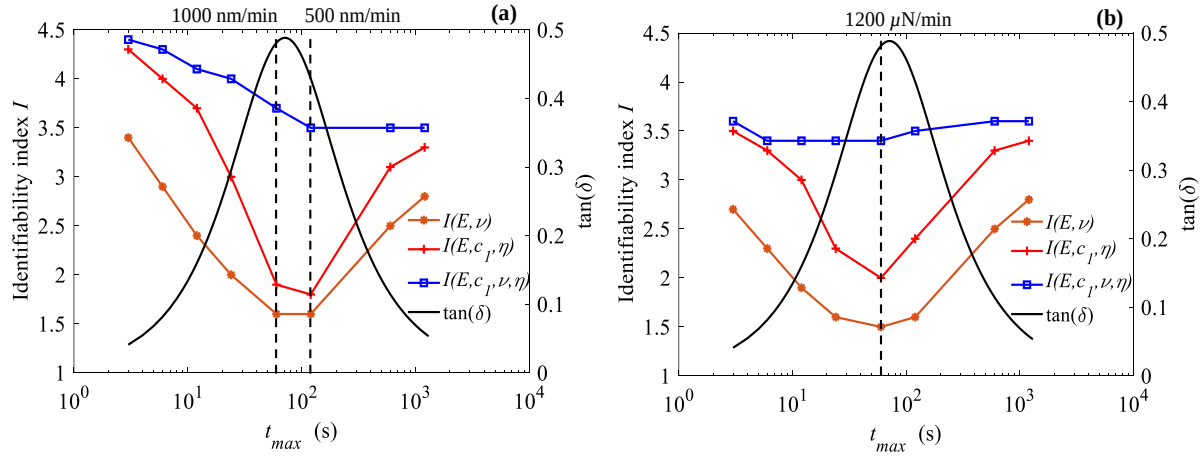

Fig. 11. I-index for the nanoindentation triangular tests and the loss factor using the solution $\widehat{\boldsymbol{\theta}}^{(5)}$ with equivalent Berkovich indenter tip, (a) displacement-controlled mode. (b) force-controlled mode.

The link between $\tan(\delta)$ and the I-index is also investigated for trapezoidal and exponential loading types using equation (Eq.16). Fig. 12 shows the I-index results for 3 combinations of material parameters with equivalent Berkovich indenter tip as function of the loss factor using the solution $\widehat{\boldsymbol{\theta}}^{(5)}$. It can be seen that, whatever the loading type, the better identifiability corresponds to conditions which maximize the loss factor. The link between $\tan(\delta)$ and the I-index depends on the nanoindentation rate to solicit the dissipative phenomena, which is different from a loading to the other.

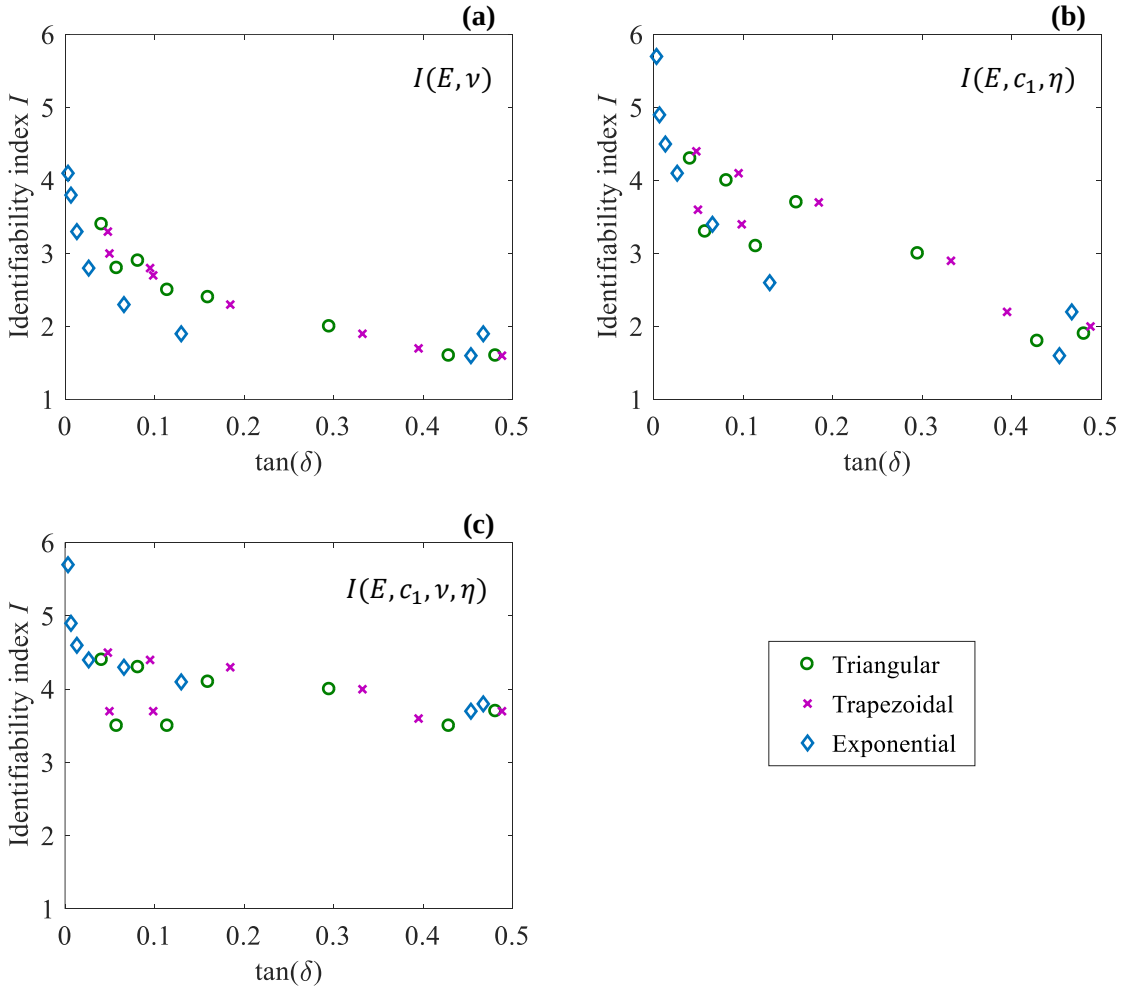

Fig. 12. I-index versus $tan(\delta)$ using three loading types with the solution $\widehat{\boldsymbol{\theta}}^{(5)}$ for three combinations of parameters, (a) $I(E,\nu)$. (b) $I(E,c_1,\eta)$. (c) $I(E,c_1,\nu,\eta)$.

3.3. Combining tests for a well-posed inverse problem

In order to determine the better identifiability of the four material parameters, the combination of numerical nanoindentation triangular tests and indenter angle tips is investigated. The combination of the equivalent 2D cube corner ($\alpha = 42.28°$) and Berkovich ($\alpha = 70.3°$) indenter tips is considered to determine a unique solution for the inverse problem.

3.3.1. Several nanoindentation triangular tests

The identifiability analysis is carried out using a set of 2 to 8 nanoindentation triangular numerical tests (50, 100, 500, 1000, 2500, 5000, 10000, 20000 nm/min) for the solution $\widehat{\boldsymbol{\theta}}^{(5)}$. Table 8 summarizes the I-index values for all subsets of nanoindentation tests. The combination of nanoindentation triangular tests decreases the maximum I-index values, and therefore improves the identification robustness. All combinations of two parameters can be identified from the subset of two nanoindentation tests. The subset of multiple nanoindentation tests allows to identify 9 combinations of parameters. The identification of the four material parameters is still impossible despite the additional information. The value of the I-index for the four material parameters is never less than 3.5. Comparing the I-index results from single nanoindentation test (Table 4) and the subset of several tests (Table 8), it is observed that the set of eight nanoindentation rates does not necessarily lead to better I-index compared to a single but properly chosen one.

Table 8. I-index for all combinations of parameters ($[I_{min}; I_{max}]$) for all subsets of nanoindentation triangular load-unload tests using the solution $\widehat{\boldsymbol{\theta}}^{(5)}$. $I \leq 2$ (green, potentially identifiable), $2 < I \leq 3$ (difficult to identify), $I > 3$ (red, not identifiable).

Combination	2 tests	3 tests	4 tests	5 tests	6 tests	7 tests	8 tests
E, c_1	[0.5; 3.9]	[0.5; 3.3]	[0.5; 2.6]	[0.5; 1.7]	[0.6; 1.2]	[0.6; 0.8]	0.7
c_1, η	[0.4; 2.3]	[0.3; 2.2]	[0.3; 1.7]	[0.3; 1.0]	[0.4; 0.9]	[0.4; 0.7]	0.6
c_1, ν	[0.5; 2.9]	[0.5; 2.4]	[0.5; 1.7]	[0.5; 1.1]	[0.5; 0.9]	[0.5; 0.8]	0.7
E, η	[1.2; 2.3]	[1.1; 2.1]	[1.2; 2.0]	[1.2; 1.8]	[1.3; 1.6]	[1.3; 1.5]	1.4
E, ν	[1.6; 3.1]	[1.6; 2.8]	[1.5; 2.5]	[1.6; 2.2]	[1.6; 2.0]	[1.7; 1.8]	1.7
ν, η	[0.7; 1.5]	[0.7; 1.3]	[0.8; 1.2]	[0.8; 1.1]	[0.8; 1.0]	[0.9; 0.9]	0.9
E, c_1, η	[1.3; 4.2]	[1.3; 3.8]	[1.3; 3.2]	[1.3; 2.1]	[1.3; 1.6]	[1.3; 1.5]	1.4
c_1, ν, η	[1.1; 3.4]	[1.1; 3.0]	[1.0; 2.3]	[1.0; 1.9]	[1.1; 1.6]	[1.2; 1.4]	1.3
E, ν, η	[1.7; 4.3]	[1.6; 4.1]	[1.6; 3.9]	[1.6; 3.1]	[1.7; 2.5]	[1.8; 2.0]	1.9
E, c_1, ν	[2.5; 4.2]	[2.4; 4.0]	[2.4; 3.6]	[2.4; 2.9]	[2.5; 2.7]	[2.5; 2.6]	2.6
E, c_1, ν, η	[3.5; 4.3]	[3.5; 4.3]	[3.5; 4.2]	[3.5; 4.1]	[3.6; 3.9]	[3.7; 3.8]	3.7

3.3.2. Dual nanoindentation

In the following, the combination of the indenter tip angles is used in order to determine the better approach to identify the four viscoelastic material properties. Table 9 presents the I-index values for all dual nanoindentation using triangular numerical test at 500 nm/min in displacement-controlled mode with the solution $\widehat{\boldsymbol{\theta}}^{(5)}$. Whatever the combination, it is possible to identify two parameters, however, for three parameters, the indenter tips have to be carefully chosen. The value of the I-index for the combination of four parameters from the combination of equivalent cube corner ($\alpha = 42.28°$) and Berkovich ($\alpha = 70.3°$) indenter tips is equal to 2. The identification of all combinations of parameters using loading and unloading phases may thus provide a unique solution. The identifiability is difficult from unloading phases and

impossible if only loading phases are considered. Fig. 13 displays the simulated *P*-*h* curves for the two indenter tips at 500 nm/min for the solution $\widehat{\boldsymbol{\theta}}^{(5)}$.

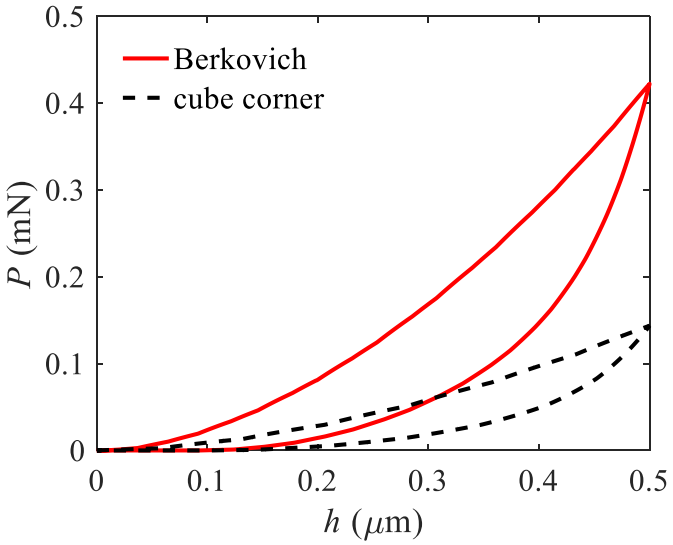

Fig. 13. Nanoindentation pseudo-experimental (*P*-*h*) curves for equivalent cube corner and Berkovich indenter tips at 500 nm/min obtained using the solution $\widehat{\boldsymbol{\theta}}^{(5)} = (E = 1.47$ GPa, $c_1 = 0.94$ GPa, $\nu = 0.4$, $\eta = 17.08$ GPa.s).

Table 9. *I*-index for all combinations of parameters for all dual nanoindentation data at 500 nm/min with the solution $\widehat{\boldsymbol{\theta}}^{(5)}$. $I \leq 2$ (green, potentially identifiable), $2 < I \leq 3$ (difficult to identify), $I > 3$ (red, not identifiable).

Combination	Dual nanoindentation $[I_{min}; I_{max}]$	Loads-unloads ($\alpha_1 = 42.28°, \alpha_2 = 70.3°$)	Loads	Unloads
E, c_1	[0.6; 0.6]	0.6	2.1	0.8
c_1, η	[0.6; 0.6]	0.6	1.8	0.8
c_1, ν	[1.1; 1.2]	1.1	1.5	1.5
E, η	[1.6; 1.6]	1.6	2.9	0.9
E, ν	[1.5; 1.6]	1.5	1.9	0.9
ν, η	[1.0; 1.1]	1.0	1.6	0.4
E, c_1, η	[1.8; 1.8]	1.8	3.0	1.7
c_1, ν, η	[1.7; 2.3]	1.7	2.1	2.0
E, ν, η	[1.7; 1.8]	1.7	3.0	1.3
E, c_1, ν	[1.9; 2.8]	1.9	2.2	2.1
E, c_1, ν, η	[2.0; 3.3]	2.0	3.1	2.1

The results of the identifiability analysis suggest that dual nanoindentation technique may provide a unique solution for the full set of four unknown parameters. Three updating processes are thus performed using equivalent cube corner and Berkovich indenter tips with the pseudo-experimental tests at 500 nm/min (Fig. 13). These updating processes make use of the three

starting points $\boldsymbol{\theta}^{(01)}$, $\boldsymbol{\theta}^{(02)}$ and $\boldsymbol{\theta}^{(03)}$. As expected from I-index results, the obtained solutions are the same for the three starting points (Table 10) and almost equal to the solution $\widehat{\boldsymbol{\theta}}^{(5)}$. The evolution of the four parameters during the algorithm iterations is illustrated in Fig. 14.

Table 10. Estimated solutions for the three starting points using dual nanoindentation.

		Parameter	Starting value	Estimated value
	j	θ_j	$\theta_j^{(0)}$	$\hat{\theta}_j$
Starting point 5: $\boldsymbol{\theta}^{(05)}$	1	E (GPa)	1.50	1.47
	2	c_1 (GPa)	12.25	0.94
	3	ν	0.4 (imposed)	0.4 (imposed)
	4	η (GPa. s)	65	17.08
Objective function $\omega^{(5)}$			4.59×10^{-2}	1.31×10^{-5}
Starting point 1: $\boldsymbol{\theta}^{(01)}$	1	E (GPa)	1.50	1.45
	2	c_1 (GPa)	12.25	0.95
	3	ν	0.4	0.39
	4	η (GPa. s)	65	17.40
Objective function $\omega^{(1)}$			8.56×10^{-1}	2.79×10^{-5}
Starting point 2: $\boldsymbol{\theta}^{(02)}$	1	E (GPa)	1.40	1.45
	2	c_1 (GPa)	8.0	0.95
	3	ν	0.3	0.39
	4	η (GPa. s)	45	17.40
Objective function $\omega^{(2)}$			4.40×10^{-1}	2.79×10^{-5}
Starting point 3: $\boldsymbol{\theta}^{(03)}$	1	E (GPa)	1.20	1.45
	2	c_1 (GPa)	4.0	0.95
	3	ν	0.2	0.39
	4	η (GPa. s)	30	17.40
Objective function $\omega^{(3)}$			1.17×10^{-1}	2.79×10^{-5}

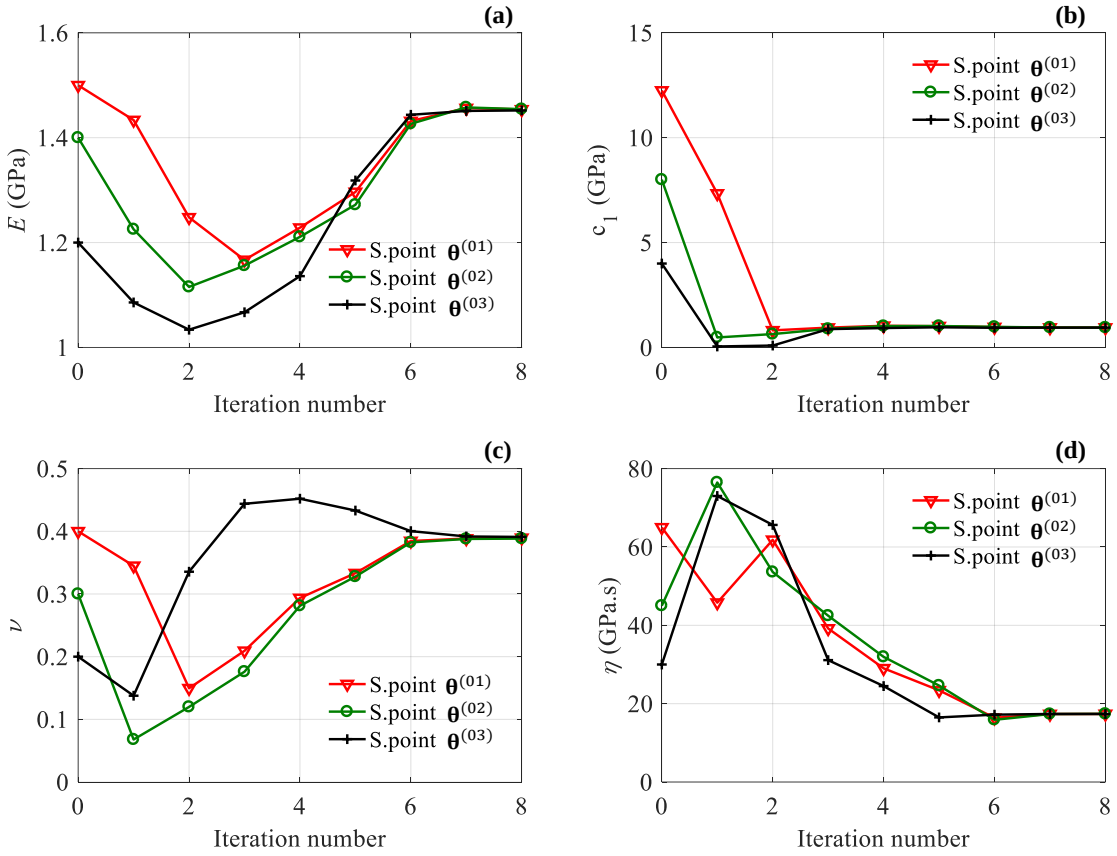

Fig. 14. Evolution of the 4 parameters (E, c_1, ν, η) during the updating process using the three starting points $\boldsymbol{\theta}^{(01)}$, $\boldsymbol{\theta}^{(02)}$ and $\boldsymbol{\theta}^{(03)}$ with dual nanoindentation technique.

The *I*-index results using two nanoindentation numerical tests performed at nanoindentation depth rate of 500 nm/min with equivalent cube corner and Berkovich indenter tips indicate that it is possible to identify the four parameters ($I(E, c_1, \nu, \eta) = 2$) (Table 9). This value of the *I*-index indicates that the inverse problem is correctly conditioned (i.e not very sensitive to noise). To illustrate the effect of noise on the updating process, a white Gaussian noise is used to disrupt the nanoindentation forces P from the numerical tests at nanoindentation depth rate of 500 nm/min using equivalent cube corner and Berkovich indenter tips. For a single test, the disrupted force $\tilde{P}$ is given by:

$$\tilde{P}(t) = P(t) + \mathcal{N}(0, s)P_{max} \tag{17}$$

where $\mathcal{N}(0, s)$ is a normal (Gaussian) distribution with zero mean and standard deviation s. P_{max} is the maximum value of the force $P(t)$.

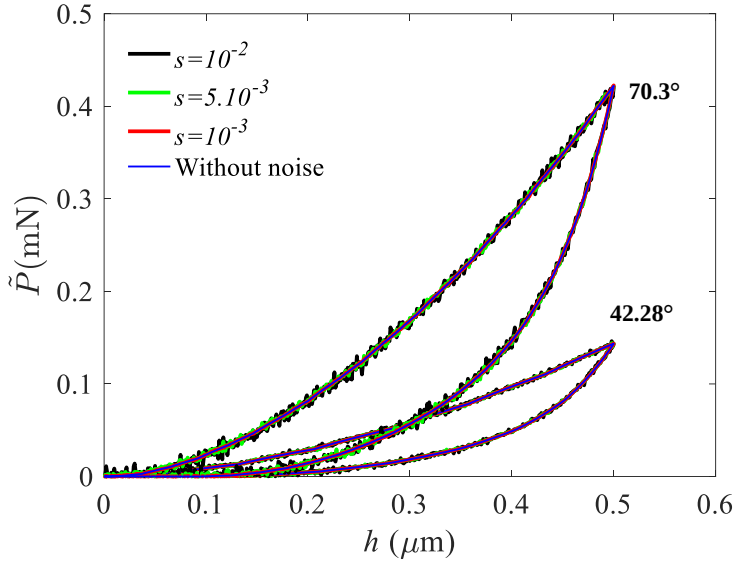

Fig. 15. Disrupted pseudo-experimental nanoindentation *P-h* curves ($\dot{h} = 500$ nm/min) for three levels of noise with equivalent cube corner and Berkovich indenter tips obtained using $\widehat{\boldsymbol{\theta}}^{(5)}$.

Both the nanoindentation forces obtained with 500 nm/min using equivalent cube corner and Berkovich indenter tips are corrupted by noise according to equation (Eq.17) (Fig. 15). The estimated solutions (Eq.6) and the uncertainties (Eq.11) for three noise standard deviations are presented in Table 11. The four material parameters tend towards the same values whatever the starting point (Fig. 16) and these values are close to the reference solution (lower than 5%). The solution is not very sensitive to this type of noise, thereby proving the proposed procedure is adequate to retrieve a unique set of viscoelastic parameters.

Table 11. Estimated solutions for the three levels of measurement noise using dual nanoindentation with the starting point $\boldsymbol{\theta}^{(02)}$. Reference $\widehat{\boldsymbol{\theta}}^{(5)} = (E = 1.47$ GPa, $c_1 = 0.94$ GPa, $\nu = 0.4$, $\eta = 17.08$ GPa.s).

	Noise		Parameter	Starting value	Estimated value	Uncertainty
	s	j	θ_j	$\theta_j^{(0)}$	$\hat{\theta}_j$	$\Delta\theta_j/\theta_j$ (%)
	10^{-2}	1	E (GPa)	1.40	1.453	29
		2	c_1 (GPa)	8.0	0.954	18
		3	ν	0.3	0.381	57
		4	η (GPa. s)	45	17.58	46
ω				4.90×10^{-2}	4.89×10^{-4}	
	5×10^{-3}	1	E (GPa)	1.40	1.460	16
		2	c_1 (GPa)	8.0	0.946	10
		3	ν	0.3	0.388	31
		4	η (GPa. s)	45	17.30	25
ω				4.96×10^{-2}	1.47×10^{-4}	

	10^{-3}	1	E (GPa)	1.40	1.453	7.5
		2	c_1 (GPa)	8.0	0.947	4.7
		3	ν	0.3	0.388	15
		4	η (GPa. s)	45	17.41	12
ω				4.94×10^{-2}	3.26×10^{-5}	
	0	1	E (GPa)	1.40	1.454	6.9
		2	c_1 (GPa)	8.0	0.947	4.3
		3	ν	0.3	0.388	14
		4	η (GPa. s)	45	17.40	11
ω				4.40×10^{-1}	2.79×10^{-5}	

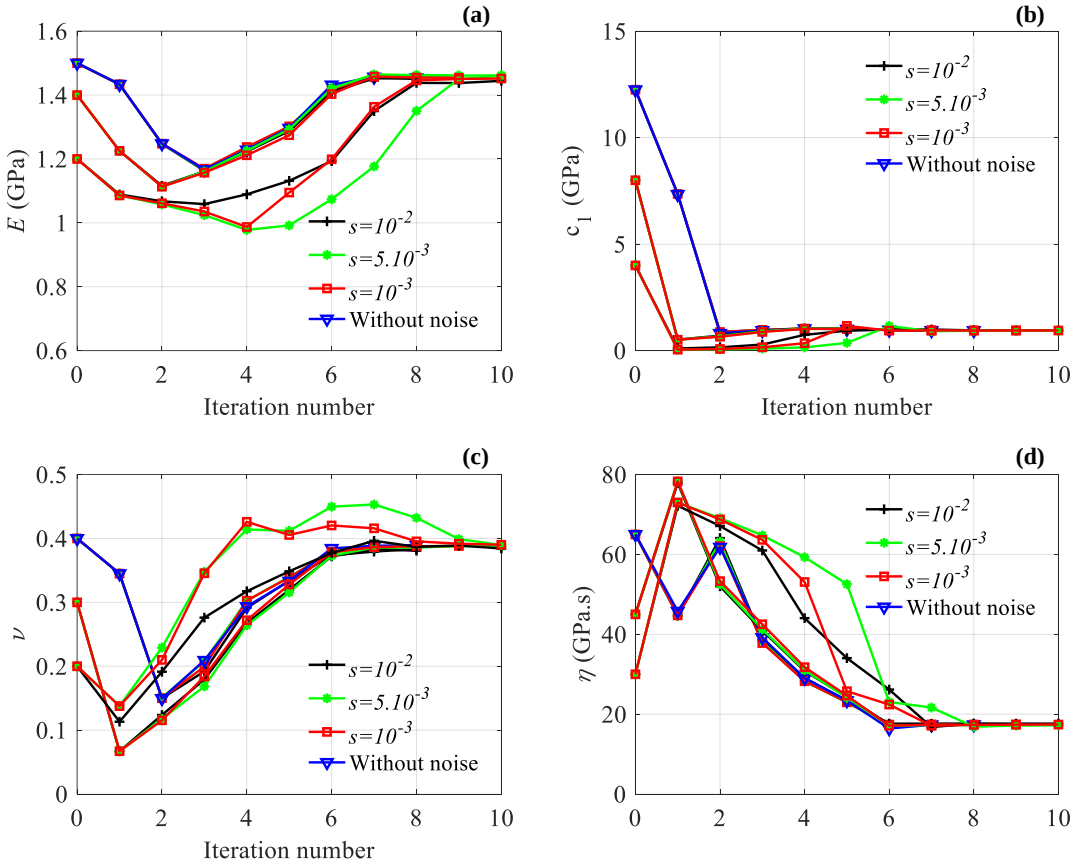

Fig. 16. Evolution of the 4 parameters (E, c_1, ν, η) during the updating process for the three starting points of the minimization algorithm $\boldsymbol{\theta}^{(01)}$, $\boldsymbol{\theta}^{(02)}$ and $\boldsymbol{\theta}^{(03)}$ using noisy force values of dual nanoindentation data.

3.4. Estimation of the viscoelastic law parameters from dual nanoindentation experimental data

In this section, two experimental nanoindentation tests ($n = 2$) carried out using the cube corner and Berkovich indenter tips at depth rate of 500 nm/min are considered. For the updating process, the starting point $\boldsymbol{\theta}^{(01)}$ is chosen to initialize the minimization algorithm. The

identified viscoelastic (VE) parameters are summarized in Table 12. Unlike the updating process using single test for the viscoelastic behavior (Table 1), the Poisson's ratio tends to the limit value ($\nu = 0.5$). The nanoindentation experimental *P-h* curves and the numerical results are plotted in Fig. 17. The results show a poor agreement between the experimental data and the updating process results.

Table 12. Estimated parameters of the viscoelastic behavior using the dual nanoindentation (cube corner and Berkovich indenter tips).

		Parameter	Starting value	Estimated value
	j	θ_j	$\theta_j^{(0)}$	$\hat{\theta}_j$
Starting point: $\boldsymbol{\theta}^{(01)}$	1	E (GPa)	1.50	1.03
	2	c_1 (GPa)	12.25	0.17
	3	ν	0.4	0.5
	4	η (GPa. s)	65	49.17
Objective function ω			2.24	6.71×10^{-2}

As it can be seen in the optical images displayed in Fig. 18, residual imprints can be observed. This is a clear indication that plasticity occurs during the indentation of PP. It thus seems necessary to assess the impact of plastic deformation on the identified VE parameters.

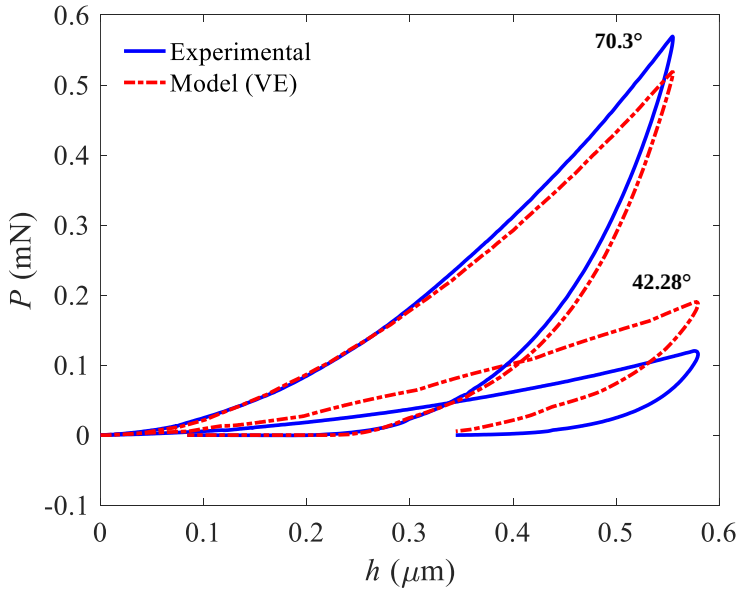

Fig. 17. Nanoindentation (*P-h*) experimental and simulated curves for the viscoelastic behavior from dual nanoindentation with cube corner and Berkovich indenter tips at 500 nm/min.

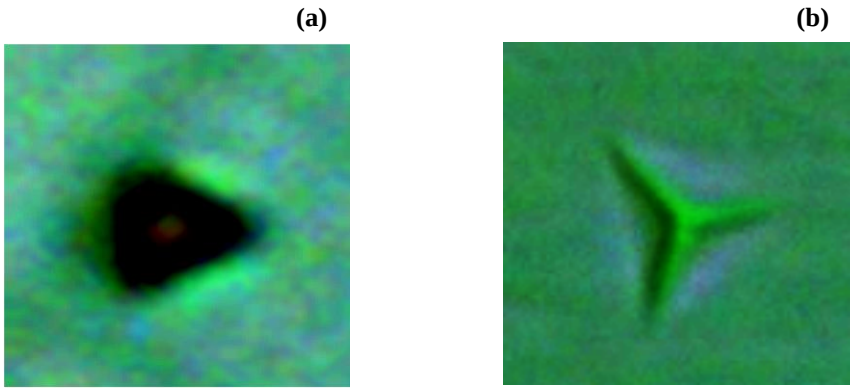

Fig. 18. Optical images of imprints on PP sample. (a) cube corner indenter tip ($2.48 \times 2.48\ \mu m^2$). (b) Berkovich indenter tip ($6.55 \times 6.55\ \mu m^2$).

3.5. Viscoelastic-plastic law

For a complete description of the material behavior, plasticity should be taken into account. In order to identify the mechanical behavior of PP, viscoelastic-plastic (VEP) behavior has been considered. In this case, the dissipation potential Ω is defined as follows:

$$\Omega = \frac{E}{2\eta}(\boldsymbol{\sigma} - \mathbf{X}^{an}) : \mathbf{S} : (\boldsymbol{\sigma} - \mathbf{X}^{an}) + \frac{1}{2K}\langle f \rangle^2 \tag{18}$$

where K is the viscosity coefficient in the viscoplastic domain. In this case, K is set to 1 MPa.s to enable the plastic deformation.

The function f is given by:

$$f(\boldsymbol{\sigma}) = \bar{\sigma} - \sigma_y \tag{19}$$

where σ_y is the yield strength and $\bar{\sigma}$ is the von Mises stress. The symbols $\langle \quad \rangle$ denote Macaulay's brackets such as $\langle f \rangle = 0$ if $f < 0$ and $\langle f \rangle = f$ if $f \geq 0$.

This viscoelastic-plastic behavior law is controlled by five material parameters, which define the parameter set $\boldsymbol{\theta} = (\theta_1, \theta_2, \theta_3, \theta_4, \theta_5) = (E, c_1, \nu, \eta, \sigma_y)$. The updating process is presented in the following paragraphs.

3.5.1. Results of the updating process for the viscoelastic-plastic law

In this case, the same dual nanoindentation tests (cube corner, Berkovich) are used and three starting points ($\boldsymbol{\theta}^{(06)}$, $\boldsymbol{\theta}^{(07)}$, $\boldsymbol{\theta}^{(08)}$) are considered (Table 13). The starting point $\boldsymbol{\theta}^{(06)}$ is built by including the yield strength of the PP (Ashby, 1994) with the estimated solution for the viscoelastic behavior $\widehat{\boldsymbol{\theta}}^{(5)}$ ($\boldsymbol{\theta}^{(06)} = (E = 1.47$ GPa, $c_1 = 0.94$ GPa, $\nu = 0.4$ (imposed), $\eta = 17.08$ GPa.s, $\sigma_y = 60$ MPa). The updating process lasts about 23 days of computation for each starting point. The minimization starting from $\boldsymbol{\theta}^{(06)}$ has been performed under the constrain $\nu = 0.4$; whereas no constrain was imposed for the starting points $\boldsymbol{\theta}^{(07)}$ and $\boldsymbol{\theta}^{(07)}$. It can be observed that the Poisson's ratio tends to the value $\nu = 0.5$ when ν is free. The parameters

E, c_1, η and σ_y tend towards different values with almost the same objective function ω for all three cases. Comparing the objective function values to that obtained for the viscoelastic law (Table 12), one can conclude that the viscoelastic-plastic law is more adequate to the description of the material behavior. Then, it is obvious that the numerical and experimental *P*-*h* curves are very close for both indenter tips (Fig. 19).

Table 13. Estimated parameters set $\widehat{\boldsymbol{\theta}}$ (Eq. 6) for the viscoelastic-plastic law using three starting points.

		Parameter	Starting value	Estimated value
	j	θ_j	$\theta_j^{(0)}$	$\hat{\theta}_j$
Starting point 6: $\boldsymbol{\theta}^{(06)}$	1	E (GPa)	1.47	1.77
	2	c_1 (GPa)	0.94	1.43
	3	ν	0.4 (imposed)	0.4 (imposed)
	4	η (GPa. s)	17.08	15.75
	5	σ_y(MPa)	60	76.70
Objective function $\omega^{(6)}$			9.78×10^{-2}	2.07×10^{-3}
Starting point 7: $\boldsymbol{\theta}^{(07)}$	1	E (GPa)	4.0	1.61
	2	c_1 (GPa)	3.0	1.31
	3	ν	0.4	0.5
	4	η (GPa. s)	60	14.41
	5	σ_y(MPa)	90	69.96
Objective function $\omega^{(7)}$			1.44	1.86×10^{-3}
Starting point 8: $\boldsymbol{\theta}^{(08)}$	1	E (GPa)	2.0	1.57
	2	c_1 (GPa)	1.5	1.32
	3	ν	0.3	0.5
	4	η (GPa. s)	40	15.25
	5	σ_y(MPa)	70	70.28
Objective function $\omega^{(8)}$			5.39×10^{-2}	1.88×10^{-3}

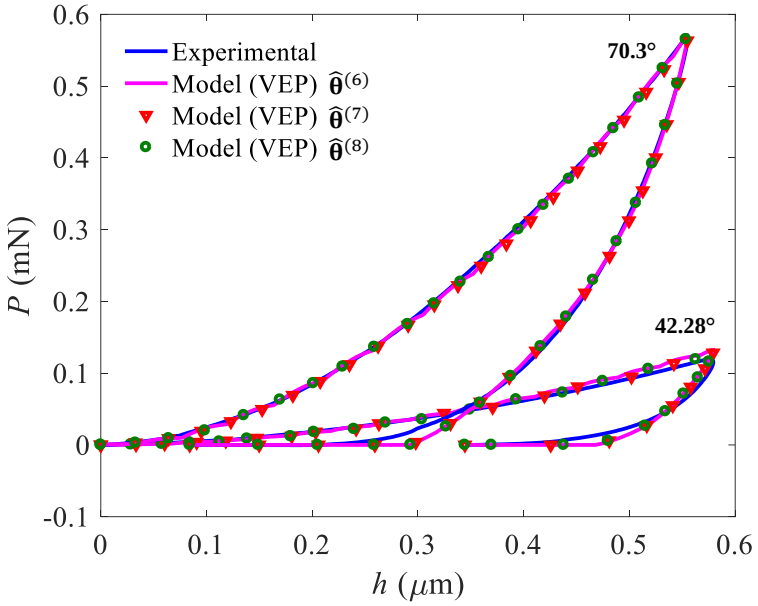

Fig. 19. Experimental ($\dot{h} = 500$ nm/min) and simulated nanoindentation *P-h* curves using cube corner and Berkovich indenter tips for the three viscoelastic-plastic solutions (Table 13).

Another updating process is also performed by imposing the yield strength $\sigma_y = 60$ MPa and the Poisson's ratio $\nu = 0.4$. The three viscoelastic parameters E, c_1 and η are estimated using the starting point: ($\boldsymbol{\theta}^{(09)} = (E = 1.47$ GPa, $c_1 = 0.94$ GPa, $\nu = 0.4$ (imposed), $\eta = 17.08$ GPa.s, $\sigma_y = 60$ MPa (imposed)). It can be observed that imposing the yield strength increases the values of the instantaneous E and anelastic c_1 moduli and decreases the viscosity coefficient η (Table 14). The obtained *P-h* curves are in good agreement with the experimental data compared to those in viscoelastic case (Fig. 20). This means that the addition of a yield strength, even when is set to a wrong value, allows a better prediction of the viscoelastic part of the PP behavior. The identifiability analysis shows that when the yield strength σ_y and Poisson's ratio ν are known, the identifiability of the three parameters E, c_1 and η is possible $I(E, c_1, \eta) = 2.0$. The identification of the five viscoelastic-plastic parameters from this dual nanoindentation is difficult ($I(E, c_1, \nu, \eta, \sigma_y) = 2.8$).

Table 15. Estimated solution for the viscoelastic-plastic law with imposing yield strength.

		Parameter	Starting value	Estimated value
	j	θ_j	$\theta_j^{(0)}$	$\hat{\theta}_j$
Starting point 9: $\boldsymbol{\theta}^{(09)}$	1	E (GPa)	1.47	1.90
	2	c_1 (GPa)	0.94	1.91
	3	ν	0.4 (imposed)	0.4 (imposed)
	4	η (GPa. s)	17.08	10.80
	5	σ_y(MPa)	60 (imposed)	60 (imposed)
Objective function $\omega^{(9)}$			9.78×10^{-2}	5.36×10^{-3}

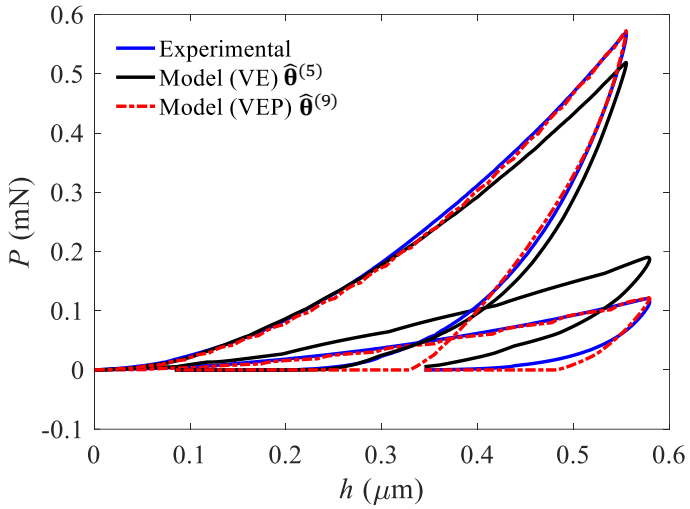

Fig. 20. Experimental ($\dot{h}$ = 500 nm/min) and simulated nanoindentation (P-h) curves with cube corner and Berkovich indenter tips for the viscoelastic and viscoelastic-plastic laws.

3.5.2. Assessment of the viscoelastic-plastic behavior

In order to validate the identified behavior, tensile tests have been performed using PP dumbbell-shaped specimens with gauge section ($20 \times 4 \times 0.5\ \text{mm}^3$). Fig. 21 shows the repetitive progressive loading test carried out at 2 N/s. The full-field strains have been measured by global digital image correlation (DIC) assuming an affine displacement field over the region of interest in both longitudinal (3) and transversal (2) directions. The comparison between the simulation results obtained using the solution $\widehat{\boldsymbol{\theta}}^{(6)} = (E = 1.77\ \text{GPa}, c_1 = 1.43\ \text{GPa}, \nu = 0.4$ (imposed), $\eta = 15.75\ \text{GPa.s}, \sigma_y = 76.70\ \text{MPa})$ and the tensile test data illustrates that the identified viscoelastic-plastic law predicts the PP behavior better than the viscoelastic one using the solution $\widehat{\boldsymbol{\theta}}^{(5)}$ (Fig. 21).

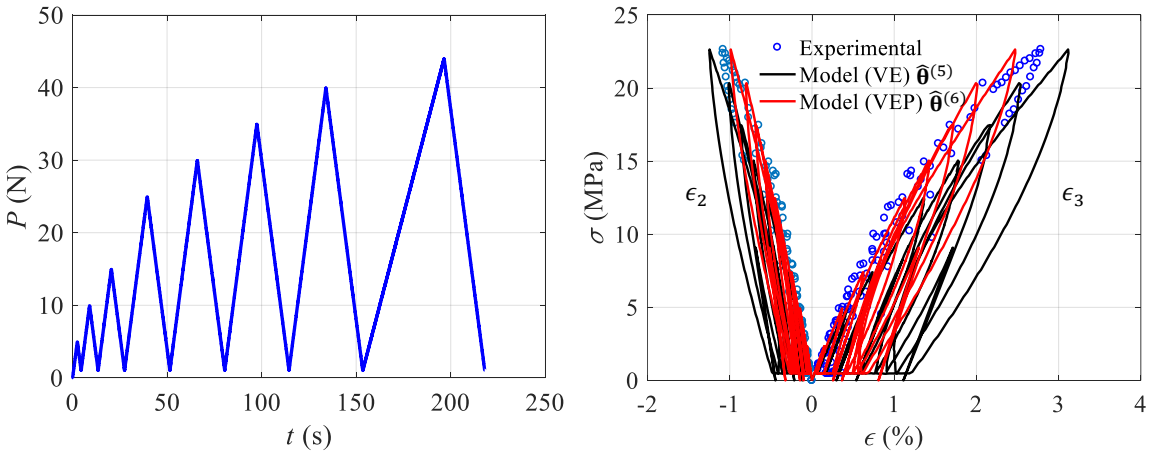

Fig. 21. Experimental data of the tensile test and simulation response using the viscoelastic and viscoelastic-plastic laws.

4. Conclusion

In this study, the uniqueness\non-uniqueness of the viscoelastic properties of polypropylene determined by the FEMU of the nanoindentation test is studied. A four-parameter viscoelastic behavior law has been implemented in a 2D axisymmetric finite element model. The FEMU process of nanoindentation test illustrates that a single nanoindentation experimental triangular load-unload test realized at constant nanoindentation depth rate ($\sim 1000\ \mathrm{nm/min}$) is not sufficient to uniquely determine the four viscoelastic properties of the material. The updating process of the FE 2D-axisymmetric model on these experimental data leads to multiple solutions for the values of the four parameters (E, c_1, ν, η) of the viscoelastic behavior law. The identification of the four parameters from a single nanoindentation triangular test is thus considered as impossible. The identifiability analysis allows the quantification of the ill-posed character of the inverse problem by a scalar I-index and shows that it is possible to identify three parameters (E, c_1, η) even if only the unloading phase is taken in account, which proves that the relevant information is in the unloading phase.

The effect of nanoindentation depth rate, loading type (triangular, trapezoidal, exponential, sinusoidal) and indenter tip angle on the identifiability is numerically investigated. The comparison between the results from the different loading types shows that the identification of the four material parameters is not possible. The included half angle α of the indenter tip does not have a significant influence on the identifiability results.

The comparison between the loss factor and the I-index results from the nanoindentation triangular tests indicates that the better identifiability of the material parameters is obtained at the maximum loss factor, which corresponds to the maximum of the dissipated energy. It is also observed that, whatever the loading type, the best identifiability is obtained if the loss factor is maximum.

The combination of several triangular load-unload tests improves the identification robustness and does not lead to better I-index for the four material parameters compared to a single but properly chosen one. We show that the combination of two numerical nanoindentation triangular tests carried out at a constant nanoindentation depth rate using equivalent cone apex angles of cube corner (42.28°) and Berkovich (70.3°) indenter tips allows for the retrieval of a unique solution of the inverse problem, which is robust with respect to the noise. The four material parameters are potentially identifiable using this experimental protocol if the material behavior is viscoelastic. These results are agree with those obtained for elastoplastic behavior.

The viscoelastic-plastic law with five parameters $(E, c_1, \nu, \eta, \sigma_y)$ improves the description of the material behavior. The identifiability results show that if the yield strength and Poisson's ratio ν are known, the identification of the three viscoelastic parameters (E, c_1, η) from dual nanoindentation experimental data (cube corner, Berkovich) is possible $(I = 2.0)$. The comparison between the simulation results of the identified viscoelastic and viscoelastic-plastic laws and the tensile test data shows that viscoelastic-plastic law is more adequate to the description of the PP behavior.

This work paves the way for the design of robust experimental protocols based on the I-index in order to identify more complex behaviors, such as the viscoelastic with non-constant Poisson's ratio, viscoelastic-plastic or viscoelastic-viscoplastic. Indeed, the I-index can be used to numerically design the nanoindentation tests which allow to activate the dissipative phenomena as much as possible, thus to identify intrinsic and reliable properties.

Acknowledgements

This work was supported by the French Ministry of Higher Education and Research. We thank P. Delobelle for his valuable scientific advice in the field of nanoindentation.

References

Alkorta, J., Martinez-Esnaola, J.M., Sevillano, J.G., 2005. Absence of one-to-one correspondence between elastoplastic properties and sharp-indentation load–penetration data. J. Mater. Res. 20, 432–437.

Ansys 16.0, 2016.

Ashby, M.F., 1994. Materials selection in mechanical design. Metall. Ital. 86, 475–475.

Boussinesq, J., 1885. Application des potentiels à l'étude de l'équilibre et du mouvement des solides élastiques: principalement au calcul des déformations et des pressions que produisent, dans ces solides, des efforts quelconques exercés sur une petite partie de leur surface ou de leur intérieur: mémoire suivi de notes étendues sur divers points de physique, mathematique et d'analyse. Gauthier-Villars.

Bucaille, J.-L., Stauss, S., Felder, E., Michler, J., 2003. Determination of plastic properties of metals by instrumented indentation using different sharp indenters. Acta Mater. 51, 1663–1678.

Capehart, T.W., Cheng, Y.T., 2003. Determining constitutive models from conical indentation: Sensitivity analysis. J. Mater. Res. 18, 827–832.

Chen, X., Ogasawara, N., Zhao, M., Chiba, N., 2007. On the uniqueness of measuring elastoplastic properties from indentation: the indistinguishable mystical materials. J. Mech. Phys. Solids 55, 1618–1660.

Chen, Z., Diebels, S., Peter, N.J., Schneider, A.S., 2013. Identification of finite viscoelasticity and adhesion effects in nanoindentation of a soft polymer by inverse method. Comput. Mater. Sci. 72, 127–139.

Cheng, L., Xia, X., Yu, W., Scriven, L.E., Gerberich, W.W., 2000. Flat-punch indentation of viscoelastic material. J. Polym. Sci. Part B Polym. Phys. 38, 10–22.

Cheng, Y.-T., Cheng, C.-M., 2004. Scaling, dimensional analysis, and indentation measurements. Mater. Sci. Eng. R Rep. 44, 91–149.

Cheng, Y.-T., Cheng, C.-M., 1999. Can stress–strain relationships be obtained from indentation curves using conical and pyramidal indenters? J. Mater. Res. 14, 3493–3496.

Constantinescu, A., Tardieu, N., 2001. On the identification of elastoviscoplastic constitutive laws from indentation tests. Inverse Probl. Eng. 9, 19–44.

Doerner, M.F., Nix, W.D., 1986. A method for interpreting the data from depth-sensing indentation instruments. J. Mater. Res. 1, 601–609.

F. Richard, 2000. MIC2M Software: Modélisation et Identification du Comportement Mécanique des Matériaux/Modeling and Identification of the Mechanical Behavior of Materials,.

Fischer-Cripps, A.C., 2011. Nanoindentation. Springer.

Gao, S.-L., Mäder, E., 2002. Characterisation of interphase nanoscale property variations in glass fibre reinforced polypropylene and epoxy resin composites. Compos. Part Appl. Sci. Manuf. 33, 559–576.

Graham, G.A., 1965. The contact problem in the linear theory of viscoelasticity. Int. J. Eng. Sci. 3, 27–46.

Guessasma, S., Sehaki, M., Lourdin, D., Bourmaud, A., 2008. Viscoelasticity properties of biopolymer composite materials determined using finite element calculation and nanoindentation. Comput. Mater. Sci. 44, 371–377.

Gujarati, D.N, 1988. Basic econometrics, 2 nd. ed. McGraw-Hill, New York.

Heinrich, C., Waas, A.M., Wineman, A.S., 2009. Determination of material properties using nanoindentation and multiple indenter tips. Int. J. Solids Struct. 46, 364–376.

Jakes, J.E., Frihart, C.R., Beecher, J.F., Moon, R.J., Stone, D.S., 2008. Experimental method to account for structural compliance in nanoindentation measurements. J. Mater. Res. 23, 1113–1127.

King, R.B., 1987. Elastic analysis of some punch problems for a layered medium. Int. J. Solids Struct. 23, 1657–1664.

Le, M.-Q., 2011. Improved reverse analysis for material characterization with dual sharp indenters. Int. J. Solids Struct. 48, 1600–1609.

Le, M.-Q., 2008. A computational study on the instrumented sharp indentations with dual indenters. Int. J. Solids Struct. 45, 2818–2835.

Lee, E.H., 1955. Stress analysis in visco-elastic bodies. Q. Appl. Math. 183–190.

Lee, E.H., Radok, J.R.M., 1960. The contact problem for viscoelastic bodies. J. Appl. Mech. 27, 438–444.

Lemaitre, J., Chaboche, J.L., 1994. Mechanics of solid materials. Cambridge university press.

Levenberg, K., 1944. A method for the solution of certain non-linear problems in least squares. Q. Appl. Math. 2, 164–168.

Liu, C.-K., Lee, S., Sung, L.-P., Nguyen, T., 2006. Load-displacement relations for nanoindentation of viscoelastic materials. J. Appl. Phys. 100, 033503.

Marquardt, D.W., 1963. An algorithm for least-squares estimation of nonlinear parameters. J. Soc. Ind. Appl. Math. 11, 431–441.

Menčík, J., He, L.H., Němeček, J., 2011. Characterization of viscoelastic-plastic properties of solid polymers by instrumented indentation. Polym. Test. 30, 101–109.

Oliver, W.C., Pharr, G.M., 2004. Measurement of hardness and elastic modulus by instrumented indentation: Advances in understanding and refinements to methodology. J. Mater. Res. 19, 3–20.

Oliver, W.C., Pharr, G.M., 1992. An improved technique for determining hardness and elastic modulus using load and displacement sensing indentation experiments. J. Mater. Res. 7, 1564–1583.

Oyen, M.L., 2006. Analytical techniques for indentation of viscoelastic materials. Philos. Mag. 86, 5625–5641.

Pac, M.-J., Giljean, S., Rousselot, C., Richard, F., Delobelle, P., 2014. Microstructural and elasto-plastic material parameters identification by inverse finite elements method of Ti (1- x) AlxN (0< x< 1) sputtered thin films from Berkovich nano-indentation experiments. Thin Solid Films 569, 81–92.

Phadikar, J.K., Bogetti, T.A., Karlsson, A.M., 2013. On the uniqueness and sensitivity of indentation testing of isotropic materials. Int. J. Solids Struct. 50, 3242–3253.

Qasmi, M., Delobelle, P., Richard, F., Brun, C., Fromm, M., 2004. Viscoelastic mechanical properties determined by nanoindentation tests and its numerical modelling of polypropylene modified by He+ particle implantation and e- irradiation. Prog. Org. Coat. 51, 195–204.

Radok, J.R.M., 1957. Visco-elastic stress analysis. Q. Appl. Math. 15, 198–202.

Richard, F., Villars, M., Thibaud, S., 2013. Viscoelastic modeling and quantitative experimental characterization of normal and osteoarthritic human articular cartilage using indentation. J. Mech. Behav. Biomed. Mater. 24, 41–52.

Tang, B., Ngan, A.H.W., 2003. Accurate measurement of tip–sample contact size during nanoindentation of viscoelastic materials. J. Mater. Res. 18, 1141–1148.

Vandamme, M., Ulm, F.-J., 2006. Viscoelastic solutions for conical indentation. Int. J. Solids Struct. 43, 3142–3165.

VanLandingham, M.R., Chang, N.-K., Drzal, P.L., White, C.C., Chang, S.-H., 2005. Viscoelastic characterization of polymers using instrumented indentation. I. Quasi-static testing. J. Polym. Sci. Part B Polym. Phys. 43, 1794–1811.

Zhang, C.Y., Zhang, Y.W., Zeng, K.Y., Shen, L., 2006. Characterization of mechanical properties of polymers by nanoindentation tests. Philos. Mag. 86, 4487–4506.